Mitogen-activated protein kinase phosphatase-1 controls PD-L1 expression by regulating type I interferon during systemic *Escherichia coli* infection

Received for publication, December 17, 2021, and in revised form, March 21, 2022 Published, Papers in Press, April 13, 2022,
https://doi.org/10.1016/j.jbc.2022.101938

Timothy J. Barley[1], Parker R. Murphy[1], Xiantao Wang[2], Bridget A. Bowman[1], Justin M. Mormol[1], Carli E. Mager[1], Sean G. Kirk[1], Charles J. Cash[1], Sarah C. Linn[3,4], Xiaomei Meng[1], Leif D. Nelin[1,5], Bernadette Chen[1,5], Markus Hafner[2], Jian Zhang[6], and Yusen Liu[1,5,*]

From the [1]Center for Perinatal Research, The Abigail Wexner Research Institute at Nationwide Children's Hospital, Columbus, Ohio, USA; [2]Laboratory of Muscle Stem Cells and Gene Regulation, National Institute of Arthritis and Musculoskeletal and Skin Disease, National Institutes of Health, Bethesda, Maryland, USA; [3]Combined Anatomic Pathology Residency/Graduate Program, Department of Veterinary Biosciences, The Ohio State University College of Veterinary Medicine, Columbus, Ohio, USA; [4]Kidney and Urinary Tract Center, The Abigail Wexner Research Institute at Nationwide Children's Hospital, Columbus, Ohio, USA; [5]Department of Pediatrics, The Ohio State University College of Medicine, Columbus, Ohio, USA; [6]Department of Pathology, University of Iowa Carver College of Medicine, Iowa City, Iowa, USA

Edited by Peter Cresswell

Mitogen-activated protein kinase phosphatase 1 (*Mkp-1*) KO mice produce elevated cytokines and exhibit increased mortality and bacterial burden following systemic *Escherichia coli* infection. To understand how *Mkp-1* affects immune defense, we analyzed the RNA-Seq datasets previously generated from control and *E. coli*–infected *Mkp-1*$^{+/+}$ and *Mkp-1*$^{-/-}$ mice. We found that *E. coli* infection markedly induced programmed death-ligand 1 (PD-L1) expression and that *Mkp-1* deficiency further amplified PD-L1 expression. Administration of a PD-L1-neutralizing monoclonal antibody (mAb) to *Mkp-1*$^{-/-}$ mice increased the mortality of the animals following *E. coli* infection, although bacterial burden was decreased. In addition, the PD-L1-neutralizing mAb increased serum interferon (IFN)-γ and tumor necrosis factor alpha, as well as lung- and liver-inducible nitric oxide synthase levels, suggesting an enhanced inflammatory response. Interestingly, neutralization of IFN-α/β receptor 1 blocked PD-L1 induction in *Mkp-1*$^{-/-}$ mice following *E. coli* infection. PD-L1 was potently induced in macrophages by *E. coli* and lipopolysaccharide *in vitro*, and *Mkp-1* deficiency exacerbated PD-L1 induction with little effect on the half-life of PD-L1 mRNA. In contrast, inhibitors of Janus kinase 1/2 and tyrosine kinase 2, as well as the IFN-α/β receptor 1–neutralizing mAb, markedly attenuated PD-L1 induction. These results suggest that the beneficial effect of type I IFNs in *E. coli*–infected *Mkp-1*$^{-/-}$ mice is, at least in part, mediated by Janus kinase/signal transducer and activator of transcription–driven PD-L1 induction. Our studies also support the notion that enhanced PD-L1 expression contributes to the bactericidal defect of *Mkp-1*$^{-/-}$ mice.

The immune defense against bacterial pathogens relies on a group of pattern recognition receptors to initiate an inflammatory response that leads to the production of inflammatory cytokines (1). Activation of these pattern recognition receptors by the conserved pathogen-associated molecular patterns, presented by the microbial pathogens, leads to a number of signal transduction cascades, such as the NF-κB, interferon (IFN) regulatory factor 3 (IRF3), and mitogen-activated protein kinase pathways, resulting in the production of a variety of cytokines, including tumor necrosis factor alpha (TNF-α) and type I IFNs (1, 2). These inflammatory cytokines can shape the development of adaptive immunity and influence the production of T-cell cytokines such as IFN-γ. The inflammatory cytokines can coordinate a multiarray of cellular programs to organize an effective immune defense against infections. For example, TNF-α and IFN-γ can induce the expression of inducible nitric oxide synthase (iNOS) to modulate the production of nitric oxide (NO) (3–5), an oxidant with strong microbicidal activity (6–8) and potent vasodilatory activity (9). Type I IFNs can induce a large number of IFN-inducible genes through the Janus kinase (JAK)/signal transducer and activator of transcription (STAT) pathway to modulate a variety of cellular activities for the restriction of pathogen replication (10, 11). Successful immune defense requires the activation of pathways that will mount an effective pathogen elimination program without triggering collateral organ damage.

Mitogen-activated protein kinase phosphatase 1 (*Mkp-1*), also referred to as dual-specificity phosphatase 1, is an inducible threonine/tyrosine protein phosphatase preferentially acting on phosphorylated p38 and c-Jun N-terminal kinase (12, 13). Both p38 and c-Jun N-terminal kinase are mitogen-activated protein kinase subfamilies critical for immune defense (14–16). *Mkp-1* is robustly induced in macrophages by a variety of pathogen-associated molecular patterns and serves as a negative regulator of the innate immune response (17–24). We have shown that upon bacterial

* For correspondence:Yusen Liu, yusen.liu@nationwidechildrens.org.

infection, *Mkp-1* KO mice produce considerably increased amounts of numerous cytokines, including TNF-α, interleukin (IL)-6, IL-10, and IFN-β (25–28). In an *Escherichia coli*–induced sepsis model, *Mkp-1*$^{-/-}$ mice produced markedly increased cytokines and exhibited elevated bacterial burden, notable metabolic abnormalities, and increased mortality relative to their WT counterparts (25, 26). We also demonstrated that neutralizing IL-10 enhanced bacterial killing (25), whereas blockade of type I IFN signaling increased mortality in *Mkp-1* KO mice, without significantly affecting bacterial loads and IL-6 levels (27). Hammer *et al.* (29) reported that *Mkp-1*/dual-specificity phosphatase 1 KO mice displayed enhanced cytokine production, impaired bacterial clearance, and increased mortality in two polymicrobial peritonitis models.

Previously, it has been reported that blockade of the immune checkpoint protein, programmed death-ligand 1 (PD-L1), enhances bacterial clearance, increases systemic inflammation, attenuates liver injury, and improves survival following cecal ligation and puncture (CLP), an experimental model of sepsis (30, 31). A clinical study also showed that PD-L1 levels correlate with increased mortality, nosocomial infection, and immune dysfunctions in septic shock patients (32). Chang *et al.* (33) demonstrated that neutralizing either PD-L1 or its receptor, programmed death-1 (PD-1), reverses sepsis-induced IFN-γ suppression, enhances major histocompatibility complex class II antigen expression on antigen-presenting cells, and improves survival in primary and secondary fungal sepsis. In the present study, we found that PD-L1 was more robustly induced in multiple organs after *E. coli* infection in *Mkp-1* KO mice than in WT mice. PD-L1 induction was almost completely blocked by an IFN-α/β receptor 1 (IFNAR1)–neutralizing monoclonal antibody (mAb), thus highlighting the critical role of type I IFN in PD-L1 induction. Interestingly, blockade of PD-L1 with a neutralizing mAb in *E. coli*–infected *Mkp-1* KO mice decreased bacterial loads but enhanced inflammation and mortality. We found that *Mkp-1* deficiency enhanced PD-L1 expression in macrophages upon *E. coli* stimulation without affecting PD-L1 mRNA stability. Finally, we showed that PD-L1 induction by *E. coli* or lipopolysaccharide (LPS) was blocked by pharmacological inhibitors of JAK1/2, tyrosine kinase 2 (TYK2), and IFNAR1-neutralizing mAb. These results suggest that *Mkp-1* controls PD-L1 expression by inhibiting type I IFN production during systemic *E. coli* infection. These studies strongly support the notion that type I IFN–mediated PD-L1 induction acts as a protective mechanism during bloodstream *E. coli* infection. These studies also revealed both beneficial (prosurvival and anti-inflammatory) and detrimental (inhibition on bacterial clearance) actions of PD-L1 during bacterial sepsis.

Results

Mkp-1$^{-/-}$ *mice exhibit significantly elevated PD-L1 expression relative to WT mice when infected with* E. coli

Previously, we performed RNA-Seq analysis on liver samples from PBS-treated control and *E. coli*–infected WT and *Mkp-1* KO mice (26). Examination of the same dataset revealed a 10.5-fold increase in PD-L1 mRNA levels in the livers of *E. coli*–infected WT mice over PBS-treated WT mice (Fig. 1*A*). While the levels of PD-L1 mRNA transcripts in PBS-treated *Mkp-1*$^{-/-}$ mice were similar to those of WT mice, *E. coli* infection in *Mkp-1*$^{-/-}$ mice resulted in a 120-fold increase in liver PD-L1 mRNA levels over PBS-treated *Mkp-1*$^{-/-}$ mice. The induction in PD-L1 mRNA by *E. coli* infection and the augmentation of PD-L1 mRNA induction by *Mkp-1* deficiency was confirmed by quantitative RT–PCR (qRT–PCR) (Fig. 1*B*). Western blot analysis indicates that PD-L1 protein levels in the livers almost mirrored the PD-L1 mRNA expression patterns: a dramatic increase in PD-L1 protein in WT mice after *E. coli* infection and further augmentation with *Mkp-1* deficiency (Fig. 1*C*). Quantitation of the PD-L1 protein levels from a large number of animals is shown in Figure 1*D*.

To characterize PD-L1 protein expression in organs, we harvested the lung, liver, spleen, heart, and kidney from control and *E. coli*–infected WT and *Mkp-1* KO mice 24 h post-infection and performed immunohistochemistry using a polyclonal antibody (Ab) against mouse PD-L1 (Fig. 2). The immunoreactivity of the Ab was confirmed by the omission of the primary Ab in the negative controls (data not shown). The most interesting features of PD-L1 expression were present in the livers and spleens. In the livers, PD-L1 protein levels were very low in both WT and *Mkp-1* KO mice without *E. coli* infection, although PD-L1 was occasionally detected on Kupffer cells (Fig. 2*A*, *left columns*). In WT mice, after *E. coli* infection, PD-L1 protein was detected on Kupffer cells, infiltrating mononuclear cells (monocytes), and sinusoid endothelial cells (Fig. 2*A*, *upper row*, *central and right columns*). In *Mkp-1* KO mice, *E. coli* infection resulted in a strong expression of PD-L1 on Kupffer cells and sinusoid endothelial cells, particularly in the centrilobular to midzonal regions (Fig. 2*A*, *lower row*, *central and right columns*). Overall, markedly more PD-L1-positive cells were seen in the livers of *E. coli*–infected *Mkp-1* KO mice than in those of *E. coli*–infected WT mice.

To quantitate the expression of PD-L1 in liver cells, we perfused the livers of control and *E. coli*–infected mice with collagenase I and enriched hepatocytes and Kupffer cells through centrifugations. The Kupffer cell–enriched and hepatocyte-enriched cell populations were stained with cell type–specific markers (F4/80 for Kupffer cells and inflammatory macrophages (34) and asialoglycoprotein receptor 1 [ASGR1] for hepatocytes) to mark these cells and assess PD-L1 expression on these cell types (Fig. 2*B*). Approximately 7.5% of the F4/80^{+} cells (Q2 and Q3 quadrants) expressed detectable levels of PD-L1 in control WT mice, and the mean fluorescent intensity (MFI) of PD-L1 staining in all F4/80^{+} cells was low. Compared with control WT mice, a larger percentage of hepatic F4/80^{+} cells (17%) in control *Mkp-1* KO mice expressed PD-L1, and the MFI of PD-L1 staining of hepatic F4/80^{+} cells was higher than that in control WT mice (155 ± 3 *versus* 285 ± 3, $p < 0.05$). *E. coli* infection markedly increased both the percentages of PD-L1-expressing cells and the MFI of PD-L1 staining in F4/80^{+} cells in both WT and *Mkp-1* KO mice. Compared with *E. coli*–infected WT mice, both the percentage of PD-L1-expressing cells and the MFI of PD-L1 staining

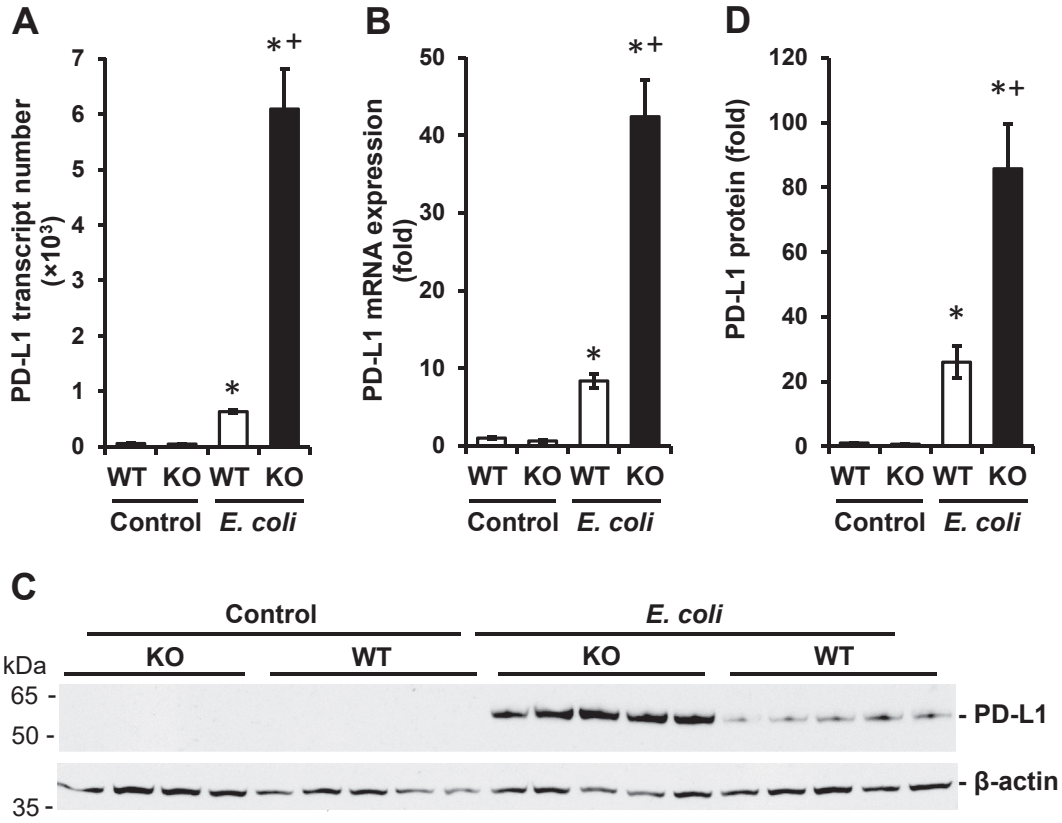

Figure 1. *Mkp-1* deficiency exacerbates PD-L1 induction in *Escherichia coli*–infected mice. WT and *Mkp-1* KO mice on a C57/129 background were infected with *E. coli* (O55:B5) i.v. at a dose of 2.5 × 10^7 CFU/g b.w. or injected with PBS (controls). Mice were euthanized after 24 h, and total RNA was isolated from the livers using Trizol for RNA-Seq analyses or qRT–PCR. The livers were homogenized to extract soluble protein for Western blot analysis. *A*, copy numbers of PD-L1 mRNA in the livers of PBS-treated or *E. coli*–infected mice determined by RNA-Seq. Data are shown as means ± SE (n = 4 mice in each group). *$p < 0.05$, compared with PBS-treated mice of the same genotype (*t* test); $^+p < 0.05$, compared with *E. coli*–infected *Mkp-1*$^{+/+}$ mice (*t* test). *B*, PD-L1 mRNA levels in the livers of PBS-treated or *E. coli*–infected mice determined by qRT–PCR. PD-L1 mRNA levels were normalized to 18S ribosomal RNA and calculated using the $2^{-\Delta\Delta CT}$ method. PD-L1 mRNA expression levels were presented as fold of changes relative to those in PBS-treated *Mkp-1*$^{+/+}$ mice. Data are shown as means ± SE (n = 4 mice in each group). *$p < 0.05$, compared with PBS-treated mice of the same genotype (*t* test); $^+p < 0.05$, compared with *E. coli*–infected *Mkp-1*$^{+/+}$ mice (*t* test). *C*, levels of PD-L1 protein in the livers of control and *E. coli*–infected mice. PD-L1 protein levels were assessed by Western blotting using a rat mAb against PD-L1 (*upper panel*). The membrane was stripped and blotted using a mouse mAb against β-actin to verify comparable loading (*lower panel*). Each lane represents an individual animal. Representative Western blotting results are shown. *D*, quantitative comparison of PD-L1 protein levels in different groups of mice. PD-L1 protein levels were expressed as fold relative to the average level in the PBS-treated WT mice. Values in the graph represent means ±SE (n = 8–10 mice in each group). *$p < 0.05$, compared with PBS-treated mice of the same genotype (*t* test). $^+p < 0.05$, compared with *E. coli*–infected WT mice (*t* test). b.w., body weight; CFU, colony-forming unit; mAb, monoclonal antibody; *Mkp-1*, mitogen-activated protein kinase phosphatase 1; PD-L1, programmed death-ligand 1; qRT–PCR, quantitative RT–PCR.

among the F4/80$^+$ cells were higher in *E. coli*–infected *Mkp-1* KO mice (40% *versus* 66%; MFI 646 ± 12 *versus* 1099 ± 16 [$p < 0.05$], respectively). However, flow cytometry analysis of ASGR1$^+$ hepatocytes did not detect a marked difference in PD-L1 expression between WT and *Mkp-1* KO mice or a convincing effect of *E. coli* infection on hepatocyte PD-L1 expression (data not shown).

In the spleens of both WT and *Mkp-1* KO mice treated with PBS, PD-L1 expression was most prominent in macrophages within the marginal zone of the white pulp (Fig. S1*A*, *left column*, *insets*) and to a lesser degree within the periarteriolar lymphoid sheath (Fig. S1*A*). *E. coli* infection moderately increased PD-L1 expression within the white pulp marginal zone (Fig. S1*A*, *central column*, *insets*) and markedly enhanced PD-L1 expression in macrophages within the red pulp (Fig. S1*A*, *right columns*). Flow cytometry analysis of splenocytes indicated that PD-L1 was increased in F4/80$^+$ macrophages upon *E. coli* infection in both WT and *Mkp-1* KO mice (Fig. S1*B*). PD-L1 expression was slightly higher in splenic F4/80$^+$ macrophages in *Mkp-1* KO mice than in F4/80$^+$ macrophages in WT mice (Fig. S1*B*). PD-L2 was slightly induced upon *E. coli* infection in splenic F4/80$^+$ macrophages in *Mkp-1* KO mice, although there was no significant difference of PD-L2 expression in F4/80$^+$ macrophages between WT and *Mkp-1* KO mice. PD-L1 expression was also increased in response to *E. coli* infection in splenic CD11c$^+$ dendritic cells, and PD-L1 appeared slightly higher in *Mkp-1*$^{-/-}$ dendritic cells than in WT dendritic cells.

In the heart, PD-L1 expression in the myocardium was very weak, although *E. coli* infection slightly enhanced PD-L1 expression in both WT and *Mkp-1* KO mice (Fig. S2, *left column*). Moderate PD-L1 expression was variably seen in myocardial capillary endothelium in both *E. coli*–infected WT and *Mkp-1* KO mice. In the lungs, PD-L1 was strongly expressed within the cell membranes of the majority of alveolar macrophages and mildly expressed in capillary and

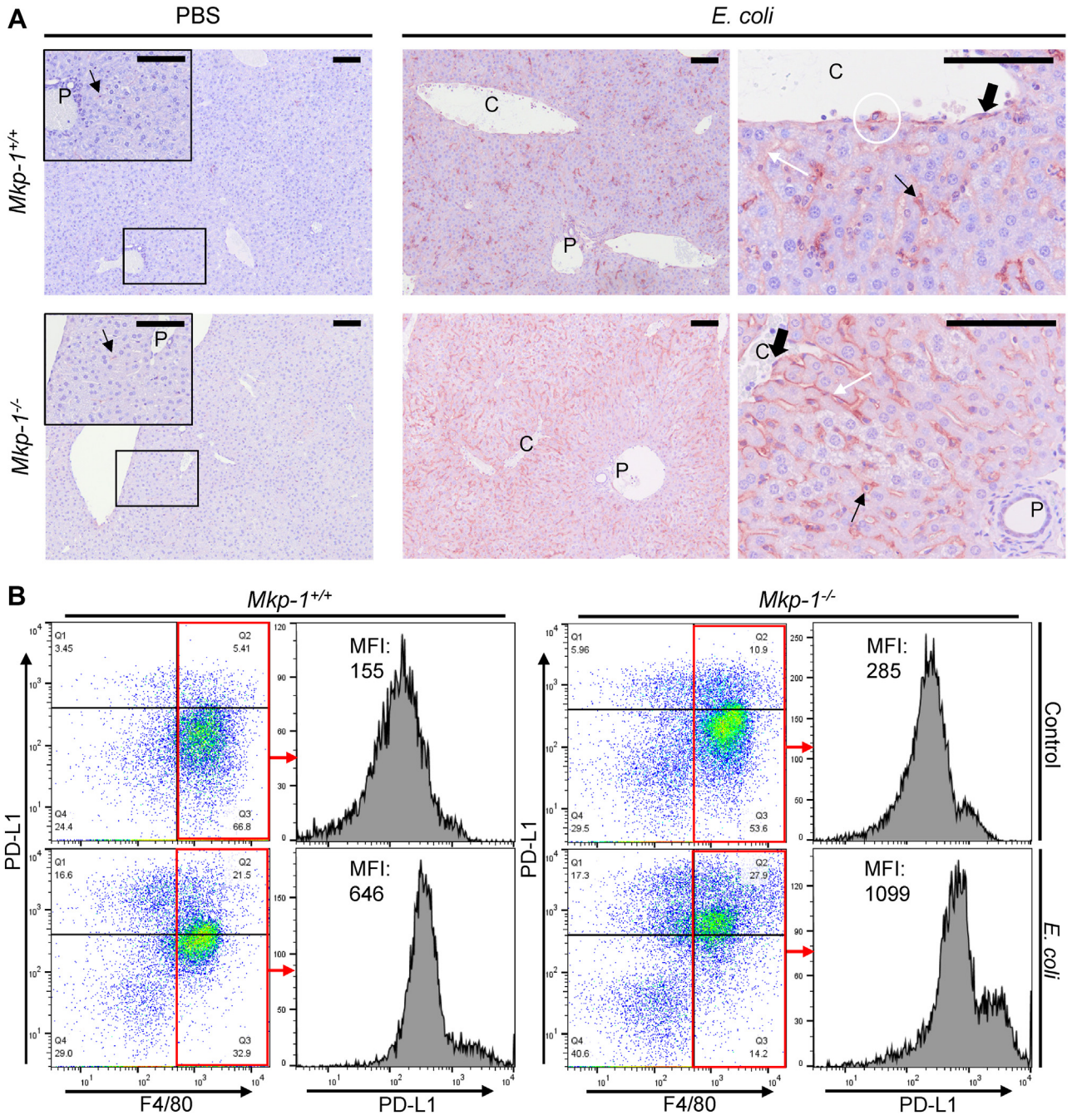

Figure 2. PD-L1 protein expression in the livers. *A*, increased PD-L1 expression in the liver of *Escherichia coli*–infected *Mkp-1*$^{-/-}$ mice compared with *Mkp-1*$^{+/+}$ mice. *Mkp-1*$^{+/+}$ and *Mkp-1*$^{-/-}$ mice (C57/129) were infected i.v. with *E. coli* at a dose of 2.8 × 10^6 CFU/g b.w. and euthanized 24 h postinfection. The organs were excised, fixed, and sectioned for immunohistochemistry with a goat polyclonal Ab against mouse PD-L1. After immunohistochemical staining, the sections were counterstained with hematoxylin. Note the marked expression in the sinusoids (*white arrows*) and Kupffer cells (*thin black arrows*) in the *E. coli*–infected *Mkp-1*$^{-/-}$ mice. The *thick black arrows* mark vessel endothelium. C = central vein, P = portal region. *Black bar* length in all images: 100 μm. Representative images from four animals are shown. *B*, flow cytometry analysis of PD-L1 expression on hepatic macrophages in control and *E. coli*–infected mice. *Mkp-1*$^{+/+}$ and *Mkp-1*$^{-/-}$ mice (C57BL6/J) (two mice per group) were infected i.v. with *E. coli* at a dose of 7.5 × 10^6 CFU/g b.w. and euthanized 24 h postinfection together with control mice. The livers were perfused and pooled to isolate enriched hepatic macrophages. The cells were stained with fluorophore-labeled F4/80 and PD-L1 mAbs and analyzed by flow cytometry. Cells were first gated on forward scatter and side scatter to exclude cell debris, and viable cells were analyzed for the expression of F4/80 and PD-L1 (first and third columns). The cell counts (*y*-axis) were plotted against PD-L1 (*x*-axis) for all F4/80$^+$ macrophages (F4/80$^+$PD-L1$^+$ and F4/80$^+$PD-L1$^-$ quadrants) in the histograms (second and fourth columns). Ab, antibody; b.w., body weight; CFU, colony-forming unit; mAb, monoclonal antibody; *Mkp-1*, mitogen-activated protein kinase phosphatase 1; PD-L1, programmed death-ligand 1.

medium caliber vascular endothelium of PBS-treated WT and *Mkp-1* KO mice (Fig. S2, *central column*). Upon *E. coli* infection, PD-L1 was strongly expressed in alveolar capillary endothelium, vascular endothelium, and monocytes adherent to the vascular endothelium (Fig. S2, *central column*). There were no overt differences in PD-L1 expression in either the lung or the heart between WT and *Mkp-1* KO mice, either treated with PBS or infected with *E. coli*. Finally, weak PD-L1

expression was observed in the kidneys of both WT and *Mkp-1* KO mice, particularly in basolateral membranes of tubular epithelium, Bowman's capsular epithelium, and small artery endothelium (Fig. S2, *right column*). *E. coli* moderately enhanced the expression of PD-L1 in both groups of mice. The induction of PD-L1 in the kidneys of *Mkp-1* KO mice appeared to be more robust than in WT mice.

Neutralization of PD-L1 in Mkp-1*-deficient mice decreases bacterial burden but enhances inflammatory response and increases mortality*

Previously, it has been reported that neutralizing PD-L1 improved bacterial clearance, increased TNF-α and IL-6, and decreased mortality in a CLP model of sepsis (30). To understand the function of PD-L1 during systemic *E. coli* infection in *Mkp-1* KO mice, we analyzed the effect of PD-L1 neutralization in these mice. Mice were first given 100 μg PD-L1-neutralizing mAb or an isotype control mAb in the late afternoon and then infected with *E. coli* the following morning. The mice were monitored for 7 days to assess animal survival (Fig. 3*A*). Compared with mice that were given the isotype control mAb, mice administered the PD-L1-neutralizing mAb had significantly greater mortality (Fig. 3*A*).

To characterize the effects of PD-L1 neutralization on the host immune responses, we harvested organs and blood from the mice 24 h postinfection to assess bacterial loads, cytokines, and tissue iNOS levels. Interestingly, we found that PD-L1 neutralization significantly decreased splenic bacterial load 24 h postinfection (Fig. 3*B*). However, the bacterial load in the blood was not significantly different between *Mkp-1* KO mice treated with the PD-L1-neutralizing mAb and those that received isotype control mAb. Serum TNF-α levels in the *Mkp-1*$^{-/-}$ mice treated with the PD-L1-neutralizing Ab were higher at 24 h postinfection than mice that received isotype control mAb (Fig. 4*A*). Serum IFN-γ and granuclocyte–macrophage colony-stimulating factor levels in the *Mkp-1*$^{-/-}$ mice treated with the PD-L1-neutralizing mAb trended higher at 24 h postinfection than mice that received isotype control mAb, whereas IL-27 levels were not different. At 48 h post *E. coli* infection, serum IFN-γ levels in the *Mkp-1*$^{-/-}$ mice treated with the PD-L1-neutralizing mAb were higher than in mice that received isotype control mAb (Fig. 4*B*), whereas TNF-α, IL-27, and granuclocyte–macrophage colony-stimulating factor levels were similar in the two groups.

NO is a potent bactericidal substance and a powerful vasodilator that has been implicated in both bacterial clearance, particularly for intracellular pathogens, and septic shock (35, 36). Excessive iNOS induction as a result of cytokine storm can lead to NO overproduction, vasodilation, hypotension, circulatory failure, and shock (36, 37). We found that iNOS expression in both the lungs and livers of *Mkp-1*$^{-/-}$ mice pretreated with PD-L1 mAb was significantly higher than in those organs of mice pretreated with the isotype control mAb (Fig. 5).

Enhanced PD-L1 expression in Mkp-1$^{-/-}$ *mice after* E. coli *infection is mediated by type I IFN*

We have previously reported that *Mkp-1*$^{-/-}$ mice produced a substantially greater amount of type I IFN than WT mice after systemic *E. coli* infection (27). In addition, type I IFN signaling plays a beneficial role for animal survival. It has been shown that both type I and type II IFNs can stimulate PD-L1 expression (38–41). To determine whether type I IFN plays a significant role in the regulation of PD-L1 in *Mkp-1*$^{-/-}$ mice after *E. coli* infection, we neutralized the receptor for type I IFN, IFNAR1, using a neutralizing mAb and assessed the expression of PD-L1 in the liver tissues. Neither WT nor *Mkp-1*$^{-/-}$ mice produced a significant amount of type I IFN, such as IFN-β, prior to *E. coli* infection (27), and PD-L1 was not detected in the livers of these mice (Fig. 6, *upper panel*, *left two lanes*). In response to *E. coli* infection, PD-L1 expression was substantially increased in mice pretreated with an isotype control mAb (Fig. 6*A*, *upper panel*, lanes 3–8), but *E. coli* infection–induced PD-L1 expression was almost completely blocked by the IFNAR1 mAb (Fig. 6, *upper panel*, lanes 9–13). These results clearly show the critical role of type I IFN in the induction of liver PD-L1 in *E. coli*–infected mice.

PD-L1 is regulated by both type I and type II IFNs *via* the JAK–STAT pathway (38, 42). Several IFN-stimulated transcription factors, including STAT1, STAT2, STAT3, IRF1, and IRF9, have been shown to regulate PD-L1 expression in a variety of cell types (38, 42–44). We mined the RNA-Seq database (26) to compare the liver mRNA expression of these transcription factors between PBS-treated and *E. coli*–infected WT and *Mkp-1* KO mice (Fig. 6*B*). All five transcription factors (STAT1, STAT2, STAT3, IRF1, and IRF9 mRNAs) were induced to various degrees by *E. coli* infection, with STAT2, STAT3, and IRF9 expression further enhanced by *Mkp-1* deficiency. These results support the notion that the JAK–STAT pathway is more robustly activated in *E. coli*–infected *Mkp-1* KO mice than in infected WT mice.

Since macrophages in both the spleens and livers strongly expressed PD-L1 following *E. coli* infection *in vivo*, we studied the regulation of PD-L1 using bone marrow–derived macrophages (BMDMs). First, we determined the effect of *Mkp-1* deficiency on PD-L1 expression in BMDM following *E. coli* stimulation by qRT–PCR over 6 h. The basal PD-L1 mRNA levels did not substantially differ between WT and *Mkp-1*$^{-/-}$ BMDM (Fig. 7*A*). Upon stimulation with heat-killed *E. coli*, PD-L1 mRNA expression was markedly induced. PD-L1 expression was more robustly induced in *Mkp-1*$^{-/-}$ BMDM than in WT BMDM, particularly after 2 h. By 6 h, PD-L1 mRNA levels were more than 60% higher in *Mkp-1*$^{-/-}$ BMDM than the WT BMDM. *Mkp-1* has been shown to regulate the stability of mRNAs that contain adenylate–uridylate-rich elements (45, 46), such as the cytokine mRNAs (47, 48). Since PD-L1 mRNA contains several putative adenylate–uridylate-rich elements (49), we assessed the mRNA stability by monitoring the decay of PD-L1 mRNA after transcriptional blockade with actinomycin D (Fig. 7*B*). The half-life of PD-L1 mRNA in *E. coli*–stimulated WT and *Mkp-1*$^{-/-}$ BMDM was

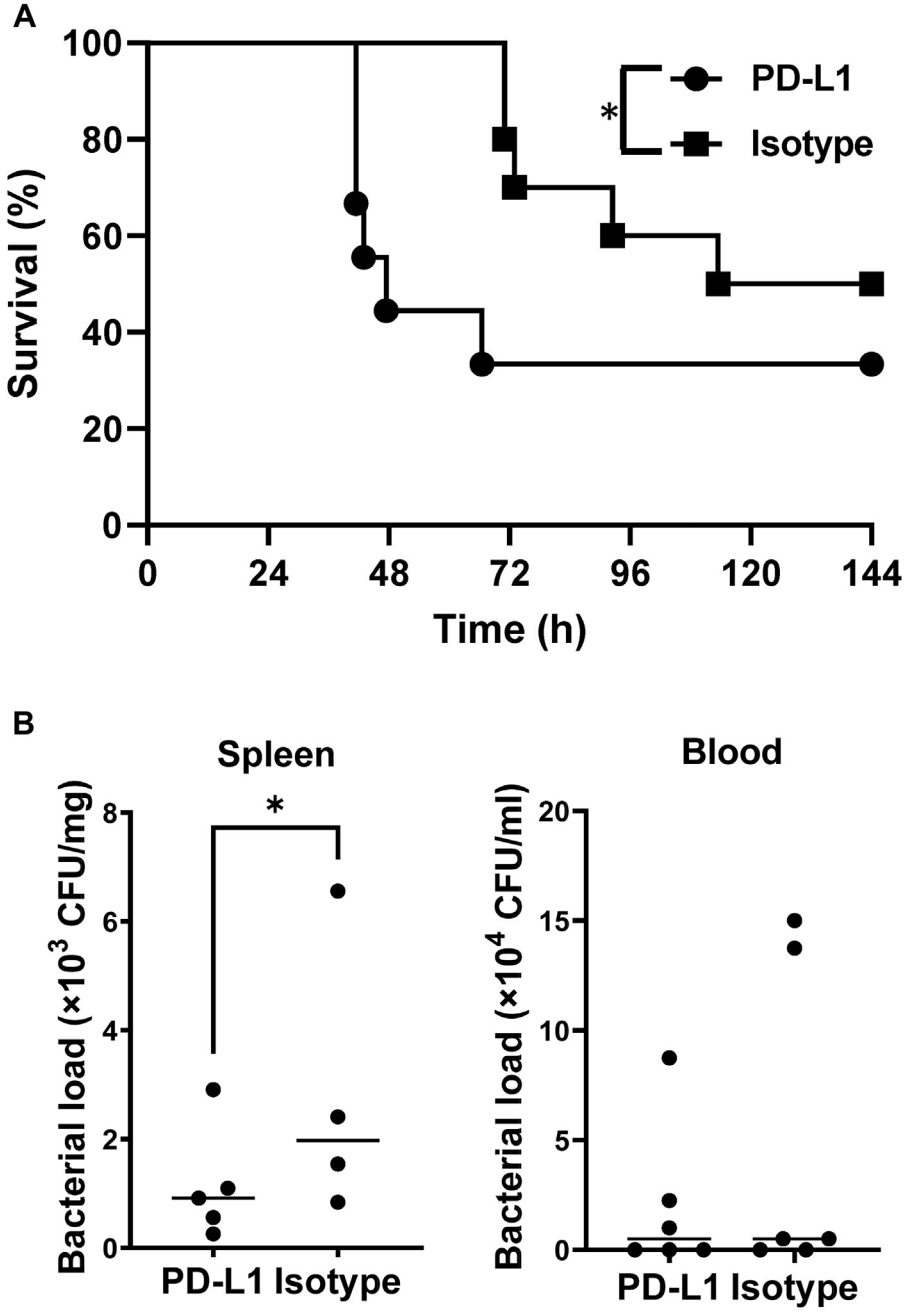

Figure 3. Neutralizing PD-L1 Ab decreases the bacterial burden but increases the mortality of *Escherichia coli*–infected *Mkp-1*$^{-/-}$ mice. *Mkp-1*$^{-/-}$ mice (C57/129) were given 100 μg of either PD-L1 mAb or an isotype control mAb i.p. About 18 h later, these mice were then infected with *E. coli* i.v. at a dose of 2.5×10^6 CFU/g b.w. The mice were monitored for 7 days to assess mortality. A group of mice were sacrificed 24 h postinfection to harvest blood and spleens aseptically for assessing bacterial burden. *A*, survival curve of *Mkp-1*$^{-/-}$ mice given either anti-PD-L1 mAb or isotype control mAb. PD-L1: n = 9; isotype control: n = 10. *$p < 0.05$ (Gehan–Breslow–Wilcoxon test). *B*, bacterial loads in the spleens and blood. Spleens harvested aseptically 24 h post-infection were homogenized. Spleen homogenates and blood samples were serially diluted and cultured on nutrient broth agar plates to quantitate CFUs. Bacterial loads in the spleens were normalized to tissue weights. Each *dot* represents an individual animal. *Horizontal line* represents mean value of CFU. *$p < 0.05$ (*t* test). Ab, antibody; b.w., body weight; CFU, colony-forming unit; mAb, monoclonal antibody; *Mkp-1*, mitogen-activated protein kinase phosphatase 1; PD-L1, programmed death-ligand 1.

similar, 4.3 and 4.6 h, respectively. These results suggest that PD-L1 mRNA expression is primarily regulated at the transcriptional level.

Macrophages are major producers of type I IFN, which activates IFNAR1 to regulate gene transcription through the STAT pathway mediated by JAK1/2 and TYK2 (50, 51). We hypothesized that *E. coli* stimulates PD-L1 expression in macrophages *via* type I IFN autocrine signaling and the JAK1/2/TYK2–STAT pathway. To test this hypothesis, we treated WT and *Mkp-1*$^{-/-}$ BMDM with LPS, a key component of *E. coli*, and assessed tyrosine-701 phosphorylation of STAT1, a key transcription factor downstream of IFNAR1 (50, 51). We confirmed that LPS more robustly induced PD-L1 expression in *Mkp-1*$^{-/-}$ BMDM than in *Mkp-1*$^{+/+}$ BMDM (Fig. 7*C*).

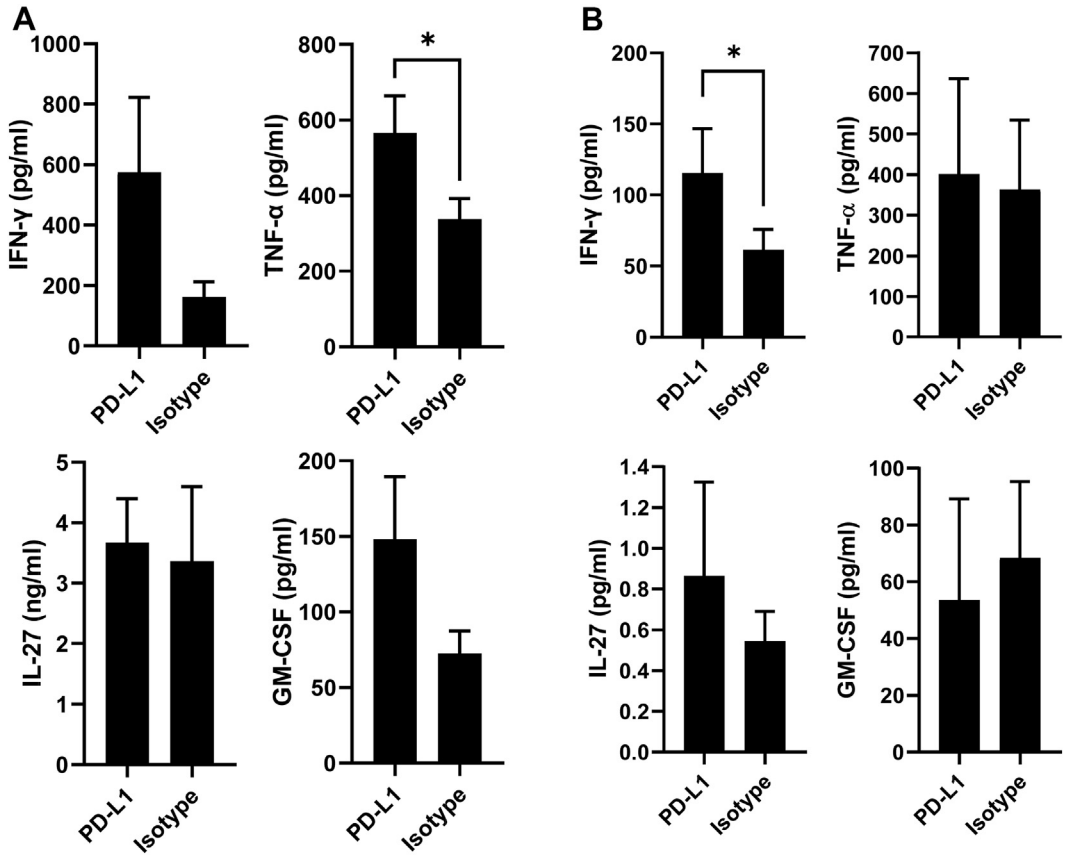

Figure 4. The effects of PD-L1 neutralization on serum cytokine levels in *Escherichia coli*–infected *Mkp-1*$^{-/-}$ mice. *Mkp-1*$^{-/-}$ mice (C57/129) were given 100 μg of either PD-L1 mAb or an isotype control mAb i.p. These mice were infected 18 h later with *E. coli* i.v. at a dose of 2.5 × 10^6 CFU/g b.w. After 24 or 48 h, these mice were sacrificed to collect blood *via* cardiac puncture and harvest different organs. Serum cytokine levels were measured using a LEGENDplex inflammation panel. Values are presented as means ± SE. *A*, cytokine concentrations at 24 h postinfection. *$p < 0.05$, Mann–Whitney test (n = 9–12 animals/group). *B*, cytokine concentrations at 48 h postinfection. *$p < 0.05$, Mann–Whitney test (n = 4–7 animals/group). b.w., body weight; CFU, colony-forming unit; mAb, monoclonal antibody; *Mkp-1*, mitogen-activated protein kinase phosphatase 1; PD-L1, programmed death-ligand 1.

Although LPS treatment of both WT and *Mkp-1*$^{-/-}$ BMDM enhanced STAT1 tyrosine phosphorylation, STAT1 phosphorylation was substantially more robust in *Mkp-1*$^{-/-}$ BMDM than in WT BMDM (Fig. 7*C*). Since STAT3 has been shown to regulate PD-L1 expression (42, 43, 52, 53), we also assessed STAT3 tyrosine phosphorylation. Unlike STAT1 phosphorylation, which reached a peak at 2 h and declined, STAT3 underwent a biphasic phosphorylation. LPS induction produced a small peak in tyrosine phosphorylation at 2 h and then declined by 4 h, followed by a stronger tyrosine phosphorylation at 24 h in *Mkp-1*$^{+/+}$ BMDM (Fig. 7*C*). Interestingly, while STAT3 tyrosine phosphorylation also displayed a biphasic course in *Mkp-1*$^{-/-}$ BMDM, phosphorylation was substantially stronger in *Mkp-1*$^{-/-}$ BMDM than in *Mkp-1*$^{+/+}$ BMDM (Fig. 7*C*). In addition, the course of STAT3 tyrosine phosphorylation was accelerated, with a second very robust STAT3 tyrosine phosphorylation seen in *Mkp-1*$^{-/-}$ at 6 h following LPS stimulation. This robust STAT3 tyrosine phosphorylation was sustained to at least 24 h. Like STAT1, JAK1 tyrosine phosphorylation following LPS stimulation occurred more robustly in *Mkp-1*$^{-/-}$ BMDM than in *Mkp-1*$^{+/+}$ BMDM (Fig. 7*C*). Likewise, TYK2 tyrosine phosphorylation also occurred more robustly in *Mkp-1*$^{-/-}$ BMDM than in *Mkp-1*$^{+/+}$ BMDM, with a course somewhat similar to JAK1 (Fig. 7*C*).

To determine the role of the IFNAR–JAK–STAT pathway in PD-L1 expression, WT and *Mkp-1*$^{-/-}$ BMDM were pretreated with a pharmacological inhibitor of JAK1/2 (Ruxolitinib [Sigma–Aldrich], a Food and Drug Administration–approved drug for myelofibrosis, polycythemia vera, and steroid-refractory acute graft-*versus*-host disease), TYK2 (Deucravacitinib [MedChemExpress], a Food and Drug Administration–approved drug for psoriasis), or with the IFNAR1-neutralizing mAb. The cells were then stimulated with *E. coli* or LPS to assess the effects of these inhibitors and the IFNAR1 blocker on PD-L1 expression (Fig. 7*D*). *E. coli* and LPS robustly induced PD-L1 expression in *Mkp-1*$^{-/-}$ BMDM. Both Ruxolitinib and Deucravacitinib potently inhibited PD-L1 induction in a dose-dependent manner. IFNAR1-neutralizing mAb also markedly inhibited PD-L1 induction by both LPS and *E. coli*. Similarly, PD-L1 induction in response to both LPS and *E. coli* in WT BMDM was also blocked by Ruxolitinib, Deucravacitinib, and IFNAR1-neutralizing mAb (Fig. S3). We also stimulated BMDM with recombinant IFN-β and assessed PD-L1 expression (Fig. 7*E*). IFN-β stimulated PD-L1 expression in both WT and *Mkp-1*$^{-/-}$ BMDM, suggesting that *Mkp-1*

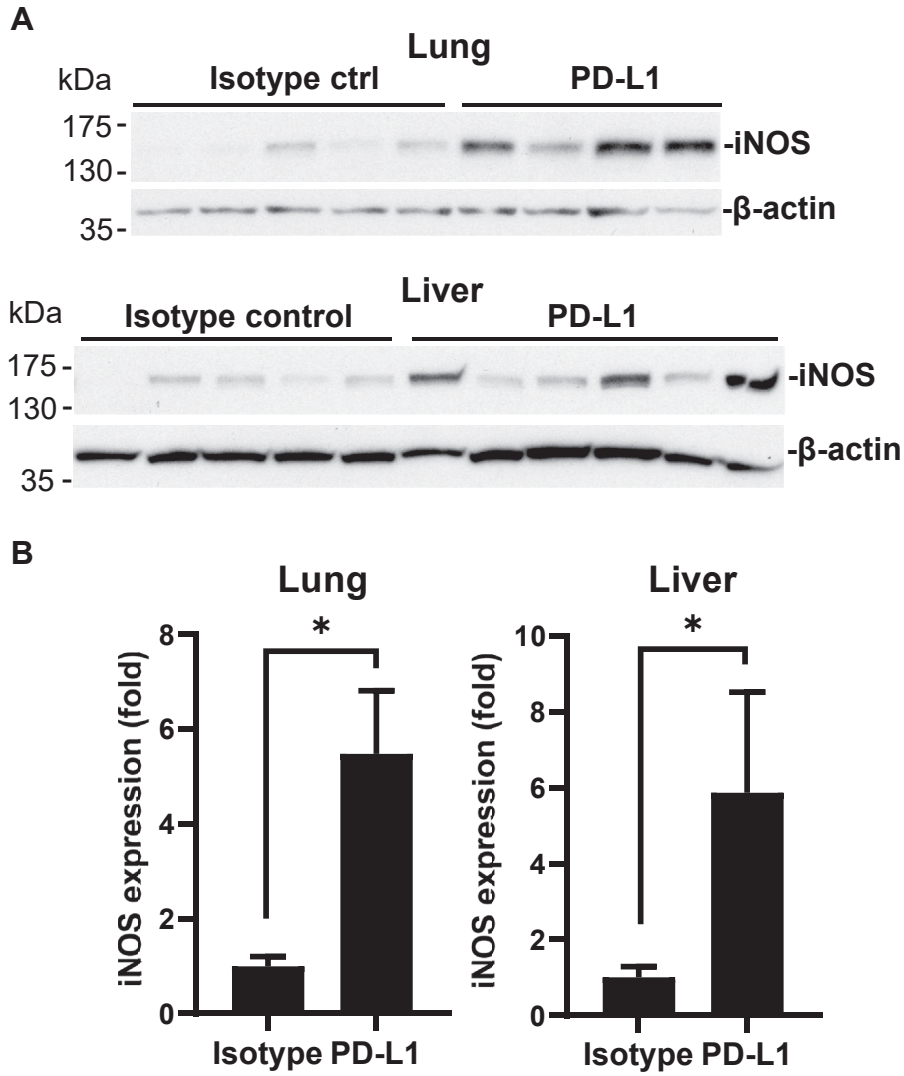

Figure 5. PD-L1 neutralization in *Escherichia coli*–infected *Mkp-1*$^{-/-}$ mice increases iNOS expression in both lungs and livers. *Mkp-1*$^{-/-}$ mice (C57/129) were first given 100 μg of PD-L1 neutralizing or isotype control mAb i.p. and then infected i.v. with *E. coli* 18 h later at a dose of 2.5 × 10^6 CFU/g b.w. Mice were sacrificed 24 h postinfection to harvest lungs and livers. Tissue homogenates were used for Western blot analysis. *A*, the effect of PD-L1 neutralization on *E. coli*–induced iNOS protein expression. iNOS protein in the lungs and livers (*upper panels*) was detected by Western blotting using a rabbit polyclonal Ab. The membranes were stripped and reblotted with a mouse β-actin mAb (*lower panels*). Results shown were representative images. *B*, quantitation of iNOS protein levels in the tissues. The iNOS protein levels were quantitated by densitometry and normalized to β-actin. iNOS protein levels were expressed as fold relative to the average value in isotype control mAb-treated animals and presented in the graphs as means ± SE (n = 5–6 animals/group). *$p < 0.05$ (*t* test). Ab, antibody; b.w., body weight; CFU, colony-forming unit; iNOS, inducible nitric oxide synthase; mAb, monoclonal antibody; *Mkp-1*, mitogen-activated protein kinase phosphatase 1; PD-L1, programmed death-ligand 1.

deficiency does not enhance the sensitivity to type I IFN. Taken together, these results strongly suggest that *E. coli* infection can induce PD-L1 expression in macrophages *via* type I IFN autocrine signaling–mediated JAK–STAT pathway.

Discussion

In this study, we found that in the absence of a functional *Mkp-1* gene, *E. coli* infection induced substantially enhanced PD-L1 expression (Fig. 1). The increase in PD-L1 expression was seen in both the livers and spleens of *E. coli*–infected *Mkp-1* KO mice (Figs. 2 and S1). Elevated PD-L1 expression was especially prominent in Kupffer cells and sinusoid endothelial cells in the liver (Fig. 2). Surprisingly, PD-L1 blockade with a neutralizing mAb significantly increased the mortality in *E. coli*–infected *Mkp-1*$^{-/-}$ mice (Fig. 3*A*), which was associated with increased tissue iNOS expression (Fig. 5) and elevated circulating TNF-α and IFN-γ at 24 and 48 h postinfection, respectively (Fig. 4). Although splenic bacterial load was decreased by PD-L1 neutralization, bacterial load in the blood was not significantly different (Fig. 3*B*). Blockade of type I IFN signaling using an IFNAR1-neutralizing mAb almost completely prevented PD-L1 induction in *E. coli*–infected *Mkp-1*$^{-/-}$ mice (Fig. 6), illustrating the pivotal role of type I IFN in PD-L1 expression. Finally, we found that *E. coli* stimulation enhanced PD-L1 mRNA expression in BMDM and

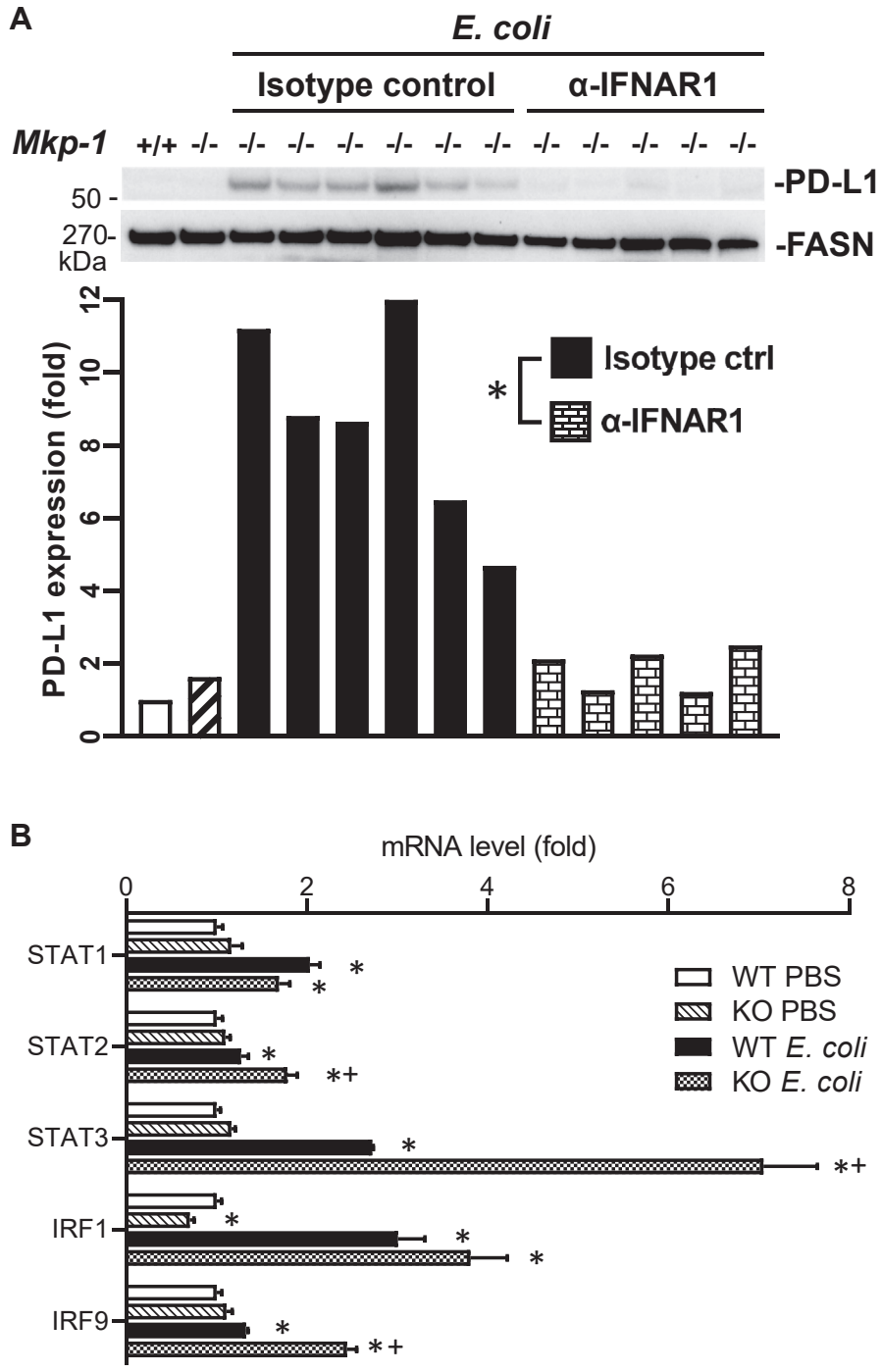

Figure 6. IFNAR1-neutralizing mAb blocks the induction of PD-L1 by *Escherichia coli* infection in *Mkp-1*$^{-/-}$ mice. *A*, the effect of IFNAR1-neutralizing mAb on *E. coli*–induced PD-L1 expression. *Mkp-1*$^{-/-}$ mice (C57/129) were first given either an antimouse IFNAR1 mAb or an isotype control (IgG1) mAb i.p. at a dose of 100 μg per mouse. After 1 h, these mice were infected i.v. with *E. coli* at a dose of 2.5×10^6 CFU/g b.w. Mice were sacrificed 24 h postinfection. Livers were excised and homogenized for Western blotting with a goat polyclonal PD-L1 Ab (*upper panel*). The membrane was stripped and blotted with a mouse mAb against FASN to verify comparable loading. The PD-L1 bands were quantitated by densitometry and normalized to the FASN bands. The values were presented in the graph as fold relative to PD-L1 level in the uninfected WT control animal. Each column corresponds to a band above. Each sample was from an individual animal. *$p < 0.05$, comparing PD-L1 protein levels between *Mkp-1*$^{-/-}$ mice given IFNAR-1 mAb and those given isotype control mAb (*t* test, n = 5–6 animals/group). *B*, the mRNA levels of selective IFN-regulated transcription factors in the livers of PBS-treated or *E. coli*–infected mice determined by RNA-Seq. Data are expressed as fold change relative to the average level in PBS-treated WT mice. Values are shown as means ± SE (n = 4 animals/group). *$p < 0.05$, compared with PBS-treated mice of the same genotype (*t* test); $^{+}p < 0.05$, compared with *E. coli*–infected *Mkp-1*$^{+/+}$ mice (*t* test). Ab, antibody; b.w., body weight; CFU, colony-forming unit; FASN, fatty acid synthase; IFN, interferon; IFNAR1, IFN-α/β receptor 1; IgG1, immunoglogulin G1; mAb, monoclonal antibody; *Mkp-1*, mitogen-activated protein kinase phosphatase 1; PD-L1, programmed death-ligand 1.

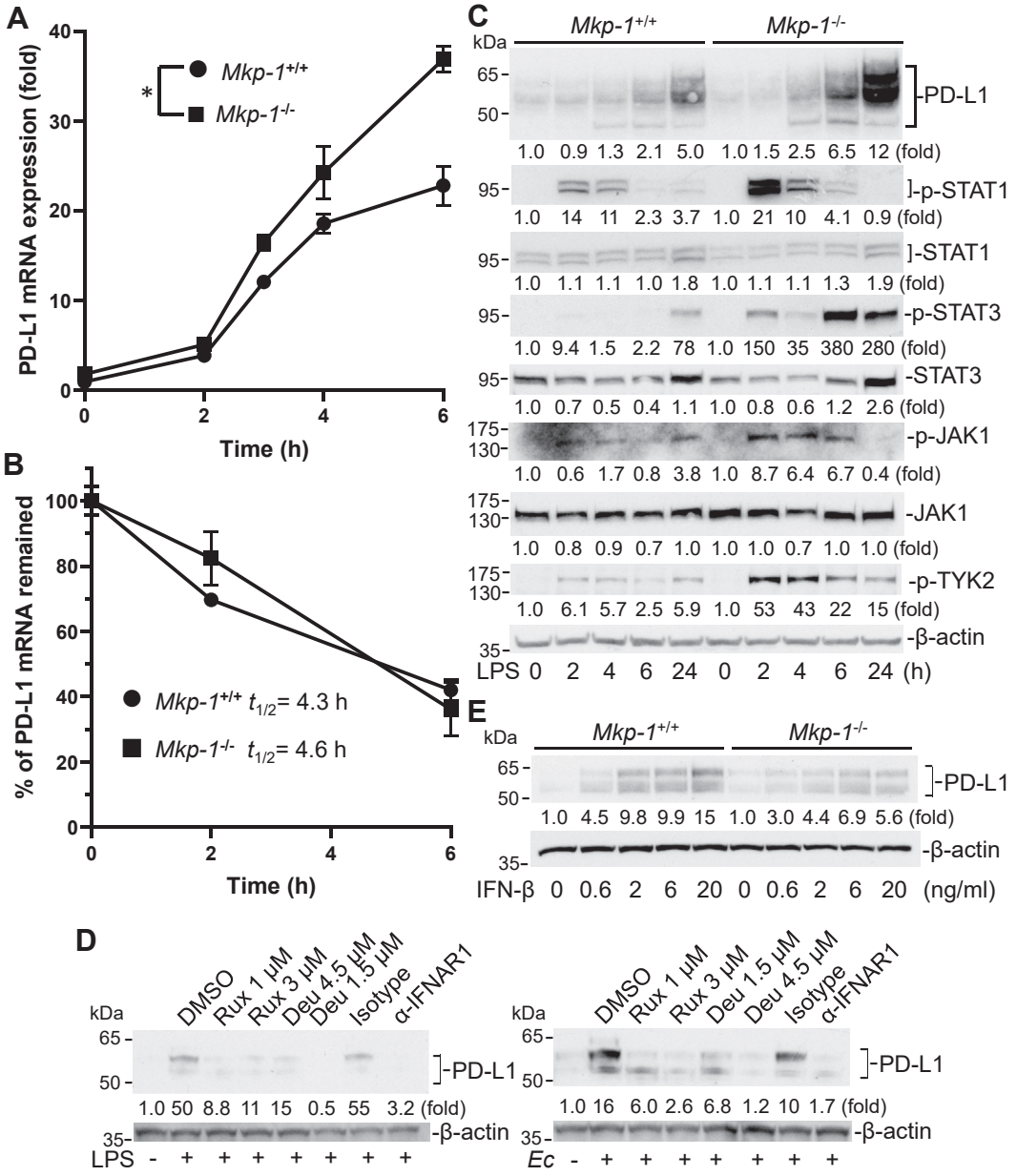

Figure 7. *Mkp-1* deficiency enhances PD-L1 mRNA expression *via* JAK–STAT pathway but has little effect on PD-L1 mRNA stability. *A*, the kinetics of PD-L1 mRNA expression in macrophages following *Escherichia coli* stimulation. *Mkp-1*$^{+/+}$ and *Mkp-1*$^{-/-}$ BMDMs were stimulated with heat-killed *E. coli* at an MOI of 10 for different times. Total RNA was isolated, and PD-L1 mRNA expression levels were assessed by qRT–PCR. The results were normalized to 18S ribosomal RNA. The expression of mRNA is presented as fold change relative to control cells. The data were shown in the graph as means ± SE (n = 9) from three separate experiments (each in triplicates). *$p < 0.05$ (two-way ANOVA). There was also an interaction between genotype and time. *B*, decay of PD-L1 mRNA in LPS-stimulated *Mkp-1*$^{+/+}$ and *Mkp-1*$^{-/-}$ BMDM following actinomycin treatment. BMDMs were first stimulated with heat-killed *E. coli* at an MOI of 10 for 4 h and then treated with 5 μg/ml actinomycin D (time 0). Cells were harvested at 0, 2, and 6 h postactinomycin treatment to isolate total RNA using Trizol. The mRNA levels at time 0 were set as 100%, and remaining RNA (%) at other time points were calculated relative to the average level of the same genotype at time 0. Data presented in the graph are means ± SE (n = 3 independent experiments). The half-life of the PD-L1 mRNA was calculated using the formulas: $N(t) = N_0\, e^{-\lambda t}$, where $\lambda = \ln 2/t_{1/2}$. *C*, time course of PD-L1 induction and tyrosine phosphorylation of STAT1, STAT3, JAK1, and TYK2 in WT and *Mkp-1*$^{-/-}$ BMDM following LPS stimulation. BMDM was treated with LPS (100 ng/ml) for the indicated times. The lysates were analyzed by Western blot analysis using a goat polyclonal PD-L1 Ab, a rabbit polyclonal Ab against phosphor-STAT1 (Tyr701) or phosphor-STAT3 (Tyr705), and a rabbit mAb against phosphor-JAK1 (Tyr1034/1035) or phosphor-TYK2 (Tyr1054/1055). Western blotting was also performed using a mouse mAb against β-actin, total STAT1, and JAK1, or a rabbit polyclonal Ab against total STAT3. *D*, the effects of JAK1/2 and TYK2 inhibitors as well as IFNAR1-neutralizing mAb on PD-L1 expression in *Mkp-1*$^{-/-}$ BMDM stimulated by LPS or *E. coli*. *Mkp-1*$^{-/-}$ BMDM was either treated with vehicle (DMSO), 1 or 3 μM of Ruxolitinib, or 1.5 or 4.5 μM of Deucravacitinib for 30 min, or treated with 10 μg/ml of isotype control mAb or 10 μg/ml IFNAR1-neutralizing mAb overnight. These cells were then treated with 100 ng/ml LPS or heat-killed *E. coli* at an MOI of 10 for 24 h. Cell lysates were subject to Western blot analysis using a goat polyclonal anti-PD-L1 antibody. The membranes were then stripped and blotted with a β-actin mAb. *E*, induction of PD-L1 by IFN-β in BMDM. *Mkp-1*$^{+/+}$ and *Mkp-1*$^{-/-}$ BMDMs were stimulated with recombinant mouse IFN-β at the indicated concentrations for 16 h. Cell lysates were analyzed by Western blotting. The protein bands of interest in the representative images shown in *C–E* were quantitated using a densitometer and normalized to β-actin. The intensities of the bands are expressed as fold relative to the unstimulated *Mkp-1*$^{+/+}$ cells and presented underneath the blot images. Western blotting images are representative results from a minimum of two independent experiments. Ab, antibody; BMDM, bone marrow–derived macrophage; DMSO, dimethyl sulfoxide; IFN, interferon; IFNAR1, IFN-α/β receptor 1; JAK, Janus kinase; LPS, lipopolysaccharide; mAb, monoclonal antibody; *Mkp-1*, mitogen-activated protein kinase phosphatase 1; MOI, multiplicity of infection; PD-L1, programmed death-ligand 1; qRT–PCR, quantitative RT–PCR; STAT, signal transducer and activator of transcription; TYK2, tyrosine kinase 2.

Mkp-1 deficiency exacerbated PD-L1 expression with little effect on PD-L1 mRNA stability (Fig. 7*A* and *B*). Like *E. coli*, LPS-induced PD-L1 was also considerably enhanced by *Mkp-1* deficiency (Fig. 7*C*). Concurrently, *Mkp-1* deficiency also potentiated LPS-induced JAK1 and TYK2 activation and elevated tyrosine phosphorylation of both STAT1 and STAT3 (Fig. 7*C*). IFNAR1 neutralization, as well as pharmacological inhibitors of JAK1/2 or TYK2, abolished PD-L1 induction (Figs. 7*D* and S3). These findings revealed a previously unknown regulation of the type I IFN/PD-L1 pathway by *Mkp-1* during immune defense. These studies also highlighted the biological functions of PD-L1 in both the inflammatory response and bactericidal actions.

The effects of PD-L1 neutralization on E. coli*–infected* Mkp-1$^{-/-}$ *mice*

PD-L1 neutralization has been shown to enhance TNF-α and IL-6 levels, decrease bacterial burden, and improve survival in a CLP model of sepsis (30, 31, 54). Similar to previous studies, we found that PD-L1 neutralization in *E. coli*–infected *Mkp-1* KO mice appeared to decrease splenic bacterial burden (Fig. 3*B*) and enhance the inflammatory response (Figs. 4 and 5); however, bloodstream bacterial load was not affected (Fig. 3*B*) while mortality was significantly increased (Fig. 3*A*). This discrepancy is likely because of the differences in the experimental sepsis model. Zhang *et al*. administered PD-L1-neutralizing mAb to WT mice and induced sepsis through CLP (30), while we infected *Mkp-1*$^{-/-}$ mice with *E. coli* i.v. It is possible that enhanced inflammatory response, as the result of PD-L1 blockade in WT mice after CLP, strengthens bacterial clearance, leading to improved survival because the inflammatory response in WT mice after CLP is likely to be less robust and damaging. Previously, we have reported that compared with WT mice, bacterial infections elicit a substantially greater inflammatory response in *Mkp-1*$^{-/-}$ mice, increasing TNF-α and IL-6 production by 7- to 10-fold (25). Here, we found that administering PD-L1-neutralizing mAb to *Mkp-1*$^{-/-}$ mice increased TNF-α and IFN-γ at 24 and 48 h post *E. coli* infection, respectively (Fig. 4), concurrent with enhanced iNOS expression in both lung and liver tissues (Fig. 5). Both TNF-α and IFN-γ can potently enhance iNOS expression (55–58). Thus, it is tempting to speculate that PD-L1 neutralization further exaggerates the hyperinflammatory response of *E. coli*–infected *Mkp-1* KO mice, leading to elevated TNF-α and IFN-γ production, potentiated iNOS induction with resultant vasodilation, and consequently, exacerbation of multiorgan failure and shock. This idea might explain why improved bacterial clearance does not translate to improved animal survival in our model. This idea is also consistent with our previous finding that killing bacteria with gentamicin completely prevented animal death in WT mice but had no effect on the mortality rate of *Mkp-1*$^{-/-}$ mice (25). Enhanced microbicidal activity as the result of enhanced inflammatory response after PD-L1/PD-1 blockade also explains why the PD-L1/PD-1 axis blockade is particularly beneficial in models of fungal sepsis (33, 59, 60). The inflammatory response after fungal infection is generally less robust, and inflammatory cytokines such as TNF-α are crucial for immune defense against fungal infections (61, 62).

Considering NO produced by iNOS is a potent bactericidal molecule, enhanced iNOS expression also helps to explain the decreased bacterial loads in the spleen of mice that received PD-L1-neutralizing mAb (Fig. 3*B*). In addition, it has been reported that PD-L1 positivity on neutrophils in septic mice is associated with compromised chemotactic activity toward chemoattractant (54). Since neutrophils are the most important leukocyte group responsible for the elimination of extracellular bacteria, it is reasonable to speculate that PD-L1 positivity on neutrophils likely would hinder neutrophil-mediated bacterial clearance. Furthermore, a recent study has shown that PD-1 blockade improves Kupffer cell–mediated bacterial clearance in an acetaminophen-induced acute liver injury model (63). The study suggests that the PD-L1–PD-1 axis exerts an inhibitory effect on the antimicrobial responses in Kupffer cells and monocytes/macrophages. Thus, it is possible that PD-L1 neutralization in septic *Mkp-1*$^{-/-}$ mice enhances neutrophil recruitment and alleviates PD-1-mediated inhibition on bactericidal actions of monocytes/macrophages to facilitate the killing of bacterial pathogens.

Previously, we have shown that blockade of the type I IFN signaling with the IFNAR1-neutralizing mAb increased mortality of *Mkp-1* KO mice following *E. coli* infection (27). These results suggest a beneficial role of the type I IFN signaling pathway in animal survival because PD-L1 expression was blocked by the IFNAR1-neutralizing mAb (Fig. 6*A*). We speculate that type I IFNs likely exert their prosurvival effects, at least in part, through upregulating PD-L1. However, there were clear distinctions; IFNAR1 neutralization had no detectable effect on TNF-α levels and bacterial loads (27), whereas PD-L1 neutralization enhanced both TNF-α and IFN-γ (Fig. 4) and decreased splenic bacterial load (Fig. 3*B*). As PD-L1 is only a small part of the IFN-stimulated genetic program, it is not surprising that IFNAR1- and PD-L1-neutralizing mAbs differentially affected cytokines and bacterial burden.

Mechanism by which Mkp-1 *deficiency enhances PD-L1 expression*

We found that PD-L1 expression in *E. coli*–infected *Mkp-1* KO mice was almost completely blocked by the IFNAR1-neutralizing mAb (Fig. 6*A*). This finding suggests that elevated type I IFNs are primarily responsible for the elevated PD-L1 expression in *E. coli*–infected *Mkp-1* KO mice. This is consistent with the observation that type I IFN–regulated key transcription factors, STAT1, STAT2, STAT3, IRF1, and IRF9, were induced in WT mice by *E. coli* infection, and *Mkp-1* deficiency exacerbated the expression of the transcription factors STAT3 and IRF1 (Fig. 6*B*). Since macrophages in both liver and spleen exhibited robust induction after *E. coli* infection, we used BMDM to study the effect of *Mkp-1* deficiency on PD-L1 expression. *Mkp-1* deficiency enhanced

PD-L1 mRNA expression following *E. coli* stimulation without affecting its mRNA stability (Fig. 7, *A* and *B*), suggesting that transcriptional induction is the primary mechanism responsible for elevated PD-L1 expression. Like heat-killed *E. coli*, LPS, a major inflammatory stimulator of *E. coli*, also strongly induced PD-L1 expression (Fig. 7*C*). We then assessed the kinetics of the JAK–STAT pathway activation by examining the tyrosine phosphorylation of JAK family TYKs, as well as STAT1 and STAT3, transcription factors known to enhance PD-L1 expression (42, 43, 52). Importantly, the activation of JAK1 and TYK2, as well as the tyrosine phosphorylation of their downstream targets STAT1 and STAT3 transcription factors, was markedly enhanced in LPS-stimulated *Mkp-1*$^{-/-}$ BMDM relative to similarly treated WT BMDM (Fig. 7*C*). Both JAK1/2 inhibitor and TYK2 inhibitor potently attenuated PD-L1 expression in both WT and *Mkp-1*$^{-/-}$ BMDM (Figs. 7*D* and S3), highlighting the critical role of the JAK–STAT pathway in PD-L1 expression. Finally, IFNAR1-neutralizing mAb also substantially inhibited PD-L1 expression (Figs. 7*D* and S3). Finally, PD-L1 is markedly induced by recombinant IFN-β in BMDM (Fig. 7*E*). These results strongly support the model that exacerbated type I IFN production following LPS stimulation in *Mkp-1*$^{-/-}$ macrophages can act in an autocrine fashion to activate the type I IFN receptors to enhance the JAK–STAT pathways, resulting in augmented PD-L1 induction. It is worth noting that the kinetics of STAT1 and STAT3 phosphorylation were very different (Fig. 7*C*). While STAT1 tyrosine phosphorylation reached a peak at 2 h and then gradually declined, STAT3 tyrosine phosphorylation occurred in a biphasic manner with initial phosphorylation occurring at 2 h, followed by a decline and then a stronger phosphorylation later. These differences suggest that STAT1 and STAT3 could be variably regulated by upstream TYKs, such as distinct members of the JAK family. Since the kinetics of JAK1 and TYK2 phosphorylation were somewhat similar and grossly mirrored the phosphorylation of STAT1, it is tempting to speculate that JAK1 and TYK2 are likely not the TYKs primarily responsible for STAT3 phosphorylation. Future studies are needed to define the TYK(s) responsible for STAT3 activation. Nonetheless, PD-L1 expression in BMDM was significantly inhibited *in vitro* by pharmacological inhibitors of JAK1/2 and TYK2, establishing the critical role of these TYKs in PD-L1 induction. The JAK–STAT pathway is activated by many cytokines whose production in response to *E. coli* is robustly enhanced as a result of *Mkp-1* deficiency, including IL-6, IL-27, and IL-10 (25, 27). The fact that IFNAR-1-neutralizing mAb alone drastically inhibited *E. coli*–induced PD-L1 expression strongly suggests that in addition to the JAK–STAT pathway, IFNAR1 also activates a unique pathway not shared with other cytokines to enhance PD-L1 expression. In summary, our studies strongly support the notion that in the absence of *Mkp-1*, higher type I IFN production leads to an augmented JAK–STAT pathway and enhanced PD-L1 induction. These findings support the idea that by regulating type I IFNs, *Mkp-1* not only shapes the innate immune response but also influences adaptive immune reactions *via* modulating PD-L1-regulated lymphocyte activities.

Experimental procedures

Experimental animals

The original *Mkp-1* KO mice on a C57/129 background (64) were obtained from Bristol Myers Squibb Pharmaceutical Research Institute. The *Mkp-1* KO mice had no overt phenotype prior to infection. Heterozygous *Mkp-1* KO mice were intercrossed to generate *Mkp-1*$^{+/+}$ and *Mkp-1*$^{-/-}$ mice for *E. coli* infection. In addition, eight generations of backcrossing of *Mkp-1*$^{+/-}$ mice to C57BL/6J mice were carried out to generate *Mkp-1*$^{-/-}$ mice on a C57BL/6J background. *Mkp-1*$^{-/-}$ and *Mkp-1*$^{+/+}$ mice on a C57BL/6J background were used for all macrophage studies *in vitro*. All mice were housed with a 12 h alternating light–dark cycle at 25 °C, with humidity between 30% and 70%, and had access to food and water ad libitum. Animals were treated humanely according to the National Institutes of Health guidelines. All experiments were preapproved by the Institutional Animal Care and Use Committee at the Abigail Wexner Research Institute at Nationwide Children's Hospital.

E. coli *infection*

A WT (smooth) strain of *E. coli* (O55:B5; American Type Culture Collection 12014) was acquired from American Type Culture Collection. Bacteria were grown in nutrient broth for 18 h at 37 °C and refreshed on the next day by culturing in new broth for 2 h after a 1:5 dilution. Bacteria were washed three times with PBS and suspended in PBS. The bacterial suspension was injected into the mouse tail veins as described previously (25, 27). Mouse survival was monitored for 7 days.

PD-L1 and IFNAR1 neutralization

Mice were given 100 μg i.p. of an *In Vivo* Plus rat antimouse PD-L1 mAb or an *In Vivo* Plus rat IgG2b isotype control mAb purchased from BioXCell. The mice were infected 18 h later i.v. with *E. coli*. Following infection, the mice were observed for mortality over a 7-day period.

In vivo IFNAR1 signaling blockade was carried out using an IFNAR1 mAb as previously described (27). Briefly, mice were first administrated with 100 μg of *In Vivo* Plus mouse anti-mouse IFNAR1 mAb or *In Vivo* Plus mouse IgG1 isotype control mAb purchased from BioXCell. After 1 h, the mice were then infected with *E. coli* i.v. and sacrificed at 24 h postinfection to assess PD-L1 expression.

Bacterial burden determination

Bacterial burden in the mice was assessed 24 h after *E. coli* infection by culture, as previously described (25). The weights of homogenized spleen tissues were used to normalize the effect of tissue sizes on bacterial counts.

Macrophage derivation, culture, and stimulation

BMDMs were generated using *Mkp-1*$^{+/+}$ and *Mkp-1*$^{-/-}$ mice on a C57BL/6J background as previously described (27). BMDMs were treated with LPS (O55:B5) (Calbiochem) or

heat-killed *E. coli* for different times to assess protein or mRNA levels. To assess the roles of IFNAR1, JAK1/2, and TYK2 in PD-L1 induction, BMDMs were pretreated with 10 μg/ml of IFNAR1-neutralizing or isotype control mAb overnight, or with a pharmacological inhibitor of either JAK1/2 (Ruxolitinib) or TYK2 (Deucravacitinib) for 30 min, and then stimulated with *E. coli* for 24 h. To assess the effect of type I IFN on PD-L1 expression in BMDM, *Mkp-1*$^{+/+}$ and *Mkp-1*$^{-/-}$ BMDMs were treated with 20 ng/ml IFN-β (BioLegend) for different times or with escalating doses of IFN-β for 16 h.

Liver RNA-Seq analysis

Mkp-1$^{+/+}$ and *Mkp-1*$^{-/-}$ mice were infected i.v. *via* tail veins with *E. coli* at a dose of 2.5×10^7 colony-forming unit/g body weight, or given 250 μl sterile PBS i.v. Animals were sacrificed 24 h later, and livers were harvested. Total RNA was isolated using Trizol (Invitrogen) from the liver tissues to perform RNA-Seq analysis (26). The RNA-Seq data have been deposited in the Gene Expression Omnibus (GSE122741) https://www.ncbi.nlm.nih.gov/geo/query/acc.cgi?acc=GSE122741. The RNA-Seq datasets were analyzed to derive mRNA expression levels in mouse livers.

qRT–PCR

Total RNA was isolated either from liver tissues or from BMDM using Trizol. RQ1 RNase-free DNase (Promega) was used to remove genomic DNA from total RNA samples prior to reverse transcription, as previously described (26, 27). PD-L1 mRNA levels were assessed by qRT–PCR using forward primer 5′-AATGCTGCCCTTCAGATCAC-3′ and reverse primer 5′-ATAACCCTCGGCCTGACATA-3′. For an internal control for normalization, 18S rRNA was quantified by qRT–PCR using primers 5′-GTAACCCGTTGAACCCCATT-3′ and 5′-CCATCCAATCGGTAGTAGCG-3′. PD-L1 mRNA expression was normalized to 18S using the $2^{-\Delta\Delta CT}$ method (36). The expression of PD-L1 mRNA in liver tissues was also assessed similarly by qRT–PCR (26).

Assessment of PD-L1 mRNA stability

To assess the effect of *Mkp-1* deficiency on PD-L1 mRNA half-life, *Mkp-1*$^{+/+}$ and *Mkp-1*$^{-/-}$ BMDMs were stimulated with heat-killed *E. coli* at a dose of 10 bacteria per macrophage for 4 h. Gene transcription was then stopped by 5 μg/ml actinomycin D, as previously described (65). RNA samples were isolated after different times, and PD-L1 mRNA expression levels were assessed by qRT–PCR. The half-life of PD-L1 mRNA was calculated using the formula $N(t) = N_0 e^{-\lambda t}$, where $\lambda = \frac{\ln 2}{t_{1/2}}$ and $t_{1/2}$ is the half-life.

Multiplex assessment for cytokines

Cytokines in the mouse serum samples were measured using a LEGENDplex multiplex kit (the mouse inflammation panel) (BioLegend), as previously described (27).

Western blot analysis and immunohistochemistry

Western blot analysis was done as described previously (19, 66). The polyclonal goat Ab against mouse PD-L1 was purchased from R&D Systems. The polyclonal iNOS Ab, the STAT1 mAb, and the mouse JAK1 mAb were purchased from Transduction Laboratories. The mouse mAb against β-actin was purchased from Sigma Chemicals. The mouse mAb against fatty acid synthase was purchased from Santa Cruz Biotechnology. Polyclonal rabbit antibodies against phosphor-STAT1 (Tyr701), phosphor-STAT3, and total STAT3, as well as the rabbit mAbs against phosphor-JAK1 (Tyr1034/1035), phosphor-TYK2 (Tyr1054/1055), and IRF-9 were purchased from Cell Signaling Technology. Quantification of protein expression was carried out by densitometry using VisionWorksLS Image Acquisition and Analysis Software (UVP), as previously described (19).

Immunohistochemistry was carried out as previously described (67). Briefly, 5 μm paraffin tissue sections were deparaffinized in xylene and rehydrated with graded ethanol to potassium–PBS solution, pH 7.2. After antigen retrieval with citrate buffer (pH 6), the sections were pretreated with 1.5% H_2O_2 for 15 min, followed by 1 h blocking with 5% normal donkey serum (Jackson ImmunoResearch). The tissues were then incubated overnight at 4 °C with a goat polyclonal Ab against the mouse PD-L1 at a concentration of 4 μg/ml diluted in 5% normal donkey serum. After 1 h incubation with biotinylated donkey antigoat immunoglobulin G at 1:600 dilution (Jackson ImmunoResearch), the sections were developed using the avidin–biotin–peroxidase system (Vectastain Elite ABC; Vector Laboratories) with Vector NovaRed (Vector Laboratories) as chromogen and hematoxylin as counterstain. The specificity of the immunoreactivity was confirmed by omission of the PD-L1 Ab. Similarly, F4/80 in organ sections was detected by immunohistochemistry, except a rat antimouse F4/80 mAb (BioXCell) and a biotinylated donkey antirat immunoglobulin G secondary Ab were used.

Flow cytometry analysis

To assess PD-L1 expression in hepatocytes and hepatic macrophages, including resident macrophages (Kupffer cells) and infiltrating inflammatory monocytes/macrophages, we isolated enriched hepatic macrophages and hepatocytes essentially as previously described (68). *E. coli*–infected and control mice were euthanized on the following day, after *E. coli* infection. The livers were perfused sequentially with Hank's balanced salt solution (Invitrogen) containing 0.5 mM EGTA and Hank's balanced salt solution containing 1 mM $CaCl_2$ and 0.64 mg/ml collagenase I (Thermo Fisher Scientific). Hepatic cells were centrifuged at 50*g* for 3 min at 4 °C. The supernatants containing macrophages were transferred to a two-layer (25%/50%) Percoll (Cytiva) density gradient and centrifuged at 1200*g* for 30 min at 4 °C. The hepatocyte-enriched cell pellets were washed three times with staining wash buffer (1× PBS, 0.1% NaN_3, and 2% fetal bovine serum). After centrifugation, the middle interphase of the Percoll gradient was collected to isolate enriched hepatic macrophages. The cells were first

incubated with a CD16/32 mAb to block the Fc receptor. Then, the enriched hepatocytes were stained with Alexa Fluor 647–conjugated ASGR1 mAb (Santa Cruz Biotechnology) and BV421-conjugated PD-L1 mAb (BioLegend). The enriched hepatic macrophages were stained with phycoerythrin (PE)-Cy7-conjugated F4/80 mAb (eBioscience) and the BV421-PD-L1 mAb. Similarly, splenocytes were stained with PerCP-Cy5.5-conjugated CD45 mAb in combination with PE-Cy7-F4/80 mAb (for macrophages) or BV510-conjugated CD11c mAb (for dendritic cells) and BV421-PD-L1 mAb or PE-conjugated PD-L2 mAb (BioLegend). After staining, the cells were washed twice with staining wash buffer and then fixed in paraformaldehyde (PBS containing 0.5% paraformaldehyde and 0.1% NaN_3). Flow cytometry was performed on a BD flow cytometer (BD Biosciences). Cells were first gated on forward scatter and side scatter to exclude cell debris, and viable cells were then gated based on cell type–specific markers, such as CD45 for leukocytes, F4/80 for macrophages, CD11c for dendritic cells, and ASGR1 for hepatocytes. PD-L1 or PD-L2 expression on these specific cell types was then assessed using FlowJo software (BD Biosciences).

Statistical analyses

GraphPad Prism 8.2.0 (GraphPad Software) was used to compare differences in gene protein expression, cytokine production, or bacterial loads between groups. The program was also utilized to identify and exclude outliers. For normally distributed datasets, an unpaired *t* test was used. For non-normally distributed data, values were either log-transformed and then compared using *t* test or directly analyzed using Mann–Whitney test. Two-way ANOVA was used to compare mRNA expression kinetics between groups over time. Differences in survival between groups were examined using Gehan–Breslow–Wilcoxon test. For all comparisons, if a *p* value is <0.05, the difference is regarded as significant.

Data availability

The RNA-Seq data have been deposited in the Gene Expression Omnibus (GSE122741) https://www.ncbi.nlm.nih.gov/geo/query/acc.cgi?acc=GSE122741.

Supporting information—This article contains supporting information.

Acknowledgments—We are grateful to Bristol–Myers Squibb Pharmaceutical Research Institute for providing *Mkp-1* KO mice. We thank Drs Xianxi Wang, Jinhui Li, Dimitrios Anastasakis, and William E. Ackerman IV for their contributions to *in vivo* infection and RNA-Seq experiments. We also gratefully acknowledge Abel J. Batty, Lisa Zhao, William M. White, and Cynthia Mcallister for technical assistance.

Author contributions—J. Z. and Y. L. conceptualization; T. J. B., X. W., J. M. M., C. E. M., S. G. K., X. M., and Y. L. methodology; L. D. N., B. C., and Y. L. formal analysis; T. J. B., P. R. M., X. W., B. A. B., J. M. M., C. E. M., S. C. L., S. G. K., and C. J. C. investigation; M. H. resources; T. J. B., P. R. M., X. W., B. A. B., J. M. M., C. E. M., S. G. K., and C. J. C. data curation; T. J. B. and Y. L. writing–original draft; B. A. B., J. M. M., C. E. M., S. C. L., L. D. N., B. C., J. Z., and Y. L. writing–review & editing; M. H. and Y. L. supervision; Y. L. project administration; L. D. N. and Y. L. funding acquisition.

Funding and additional information—This work was supported by grants from the National Institutes of Health (grant nos.: AI124029 and AI142885 [to Y. L.] and AI121196 and AI123253 [to J. Z.]). S. C. L. is supported by a Genentech Veterinary Pathology Fellowship through Genentech, Inc and The Ohio State University. The content is solely the responsibility of the authors and does not necessarily represent the official views of the National Institutes of Health.

Conflict of interest—The authors declare that they have no conflicts of interest with the contents of this article.

Abbreviations—The abbreviations used are: Ab, antibody; ASGR1, asialoglycoprotein receptor 1; BMDM, bone marrow–derived macrophage; CLP, cecal ligation and puncture; IFN, interferon; IFNAR1, IFN-α/β receptor 1; IL, interleukin; iNOS, inducible nitric oxide synthase; IRF, IFN regulatory factor; JAK, Janus kinase; LPS, lipopolysaccharide; mAb, monoclonal antibody; MFI, mean fluorescent intensity; *Mkp*, mitogen-activated protein kinase phosphatase; NO, nitric oxide; PD-1, programmed death-1; PD-L1, programmed death-ligand 1; PE, phycoerythrin; qRT–PCR, quantitative RT–PCR; STAT, signal transducer and activator of transcription; TNF-α, tumor necrosis factor alpha; TYK2, tyrosine kinase 2.

References

1. Medzhitov, R., and Janeway, C., Jr. (2000) Innate immune recognition: Mechanisms and pathways. *Immunol. Rev.* **173**, 89–97
2. Janeway, C. A., Jr., Travers, P., Walport, M., and Shlomchik, M. J. (2001) *Immunobiology: The Immune System in Health and Disease*, Garland Publishing, NY
3. Salkowski, C. A., Detore, G., McNally, R., van Rooijen, N., and Vogel, S. N. (1997) Regulation of inducible nitric oxide synthase messenger RNA expression and nitric oxide production by lipopolysaccharide *in vivo*: The roles of macrophages, endogenous IFN-gamma, and TNF receptor-1-mediated signaling. *J. Immunol.* **158**, 905–912
4. Wang, S. D., Huang, K. J., Lin, Y. S., and Lei, H. Y. (1994) Sepsis-induced apoptosis of the thymocytes in mice. *J. Immunol.* **152**, 5014–5021
5. Martin, E., Nathan, C., and Xie, Q. W. (1994) Role of interferon regulatory factor 1 in induction of nitric oxide synthase. *J. Exp. Med.* **180**, 977–984
6. McMullin, B. B., Chittock, D. R., Roscoe, D. L., Garcha, H., Wang, L., and Miller, C. C. (2005) The antimicrobial effect of nitric oxide on the bacteria that cause nosocomial pneumonia in mechanically ventilated patients in the intensive care unit. *Respir. Care* **50**, 1451–1456
7. Kono, Y., Shibata, H., Adachi, K., and Tanaka, K. (1994) Lactate-dependent killing of Escherichia coli by nitrite plus hydrogen peroxide: A possible role of nitrogen dioxide. *Arch. Biochem. Biophys.* **311**, 153–159
8. Matziouridou, C., Rocha, S. D. C., Haabeth, O. A., Rudi, K., Carlsen, H., and Kielland, A. (2018) iNOS- and NOX1-dependent ROS production maintains bacterial homeostasis in the ileum of mice. *Mucosal Immunol.* **11**, 774–784
9. Landry, D. W., and Oliver, J. A. (2001) The pathogenesis of vasodilatory shock. *N. Engl. J. Med.* **345**, 588–595
10. Bogdan, C. (2000) The function of type I interferons in antimicrobial immunity. *Curr. Opin. Immunol.* **12**, 419–424
11. Boxx, G. M., and Cheng, G. (2016) The roles of type I interferon in bacterial infection. *Cell Host. Microbe* **19**, 760–769

12. Keyse, S. M. (2000) Protein phosphatases and the regulation of mitogen-activated protein kinase signalling. *Curr. Opin. Cell Biol.* **12**, 186–192
13. Franklin, C. C., and Kraft, A. S. (1997) Conditional expression of the mitogen-activated protein kinase (MAPK) phosphatase MKP-1 preferentially inhibits p38 MAPK and stress-activated protein kinase in U937 cells. *J. Biol. Chem.* **272**, 16917–16923
14. Dong, C., Davis, R. J., and Flavell, R. A. (2002) MAP kinases in the immune response. *Annu. Rev. Immunol.* **20**, 55–72
15. Dong, C., Yang, D. D., Tournier, C., Whitmarsh, A. J., Xu, J., Davis, R. J., and Flavell, R. A. (2000) JNK is required for effector T-cell function but not for T-cell activation. *Nature* **405**, 91–94
16. Arthur, J. S., and Ley, S. C. (2013) Mitogen-activated protein kinases in innate immunity. *Nat. Rev. Immunol.* **13**, 679–692
17. Liu, Y., Shepherd, E. G., and Nelin, L. D. (2007) MAPK phosphatases–regulating the immune response. *Nat. Rev. Immunol.* **7**, 202–212
18. Lang, R., Hammer, M., and Mages, J. (2006) DUSP meet immunology: Dual specificity MAPK phosphatases in control of the inflammatory response. *J. Immunol.* **177**, 7497–7504
19. Shepherd, E. G., Zhao, Q., Welty, S. E., Hansen, T. N., Smith, C. V., and Liu, Y. (2004) The function of mitogen-activated protein kinase phosphatase-1 in peptidoglycan-stimulated macrophages. *J. Biol. Chem.* **279**, 54023–54031
20. Zhao, Q., Shepherd, E. G., Manson, M. E., Nelin, L. D., Sorokin, A., and Liu, Y. (2005) The role of mitogen-activated protein kinase phosphatase-1 in the response of alveolar macrophages to lipopolysaccharide: Attenuation of proinflammatory cytokine biosynthesis *via* feedback control of p38. *J. Biol. Chem.* **280**, 8101–8108
21. Zhao, Q., Wang, X., Nelin, L. D., Yao, Y., Matta, R., Manson, M. E., Baliga, R. S., Meng, X., Smith, C. V., Bauer, J. A., Chang, C. H., and Liu, Y. (2006) MAP kinase phosphatase 1 controls innate immune responses and suppresses endotoxic shock. *J. Exp. Med.* **203**, 131–140
22. Hammer, M., Mages, J., Dietrich, H., Servatius, A., Howells, N., Cato, A. C., and Lang, R. (2006) Dual specificity phosphatase 1 (DUSP1) regulates a subset of LPS-induced genes and protects mice from lethal endotoxin shock. *J. Exp. Med.* **203**, 15–20
23. Chi, H., Barry, S. P., Roth, R. J., Wu, J. J., Jones, E. A., Bennett, A. M., and Flavell, R. A. (2006) Dynamic regulation of pro- and anti-inflammatory cytokines by MAPK phosphatase 1 (MKP-1) in innate immune responses. *Proc. Natl. Acad. Sci. U. S. A.* **103**, 2274–2279
24. Salojin, K. V., Owusu, I. B., Millerchip, K. A., Potter, M., Platt, K. A., and Oravecz, T. (2006) Essential role of MAPK phosphatase-1 in the negative control of innate immune responses. *J. Immunol.* **176**, 1899–1907
25. Frazier, W. J., Wang, X., Wancket, L. M., Li, X. A., Meng, X., Nelin, L. D., Cato, A. C., and Liu, Y. (2009) Increased inflammation, impaired bacterial clearance, and metabolic disruption after gram-negative sepsis in Mkp-1-deficient mice. *J. Immunol.* **183**, 7411–7419
26. Borchers, A., and Pieler, T. (2010) Programming pluripotent precursor cells derived from Xenopus embryos to generate specific tissues and organs. *Genes (Basel)* **1**, 413–426
27. Kirk, S. G., Murphy, P. R., Wang, X., Cash, C. J., Barley, T. J., Bowman, B. A., Batty, A. J., Ackerman, W. E.t., Zhang, J., Nelin, L. D., Hafner, M., and Liu, Y. (2021) Knockout of MAPK phosphatase-1 exaggerates type I IFN response during systemic Escherichia coli infection. *J. Immunol.* **206**, 2966–2979
28. Wang, X., Meng, X., Kuhlman, J. R., Nelin, L. D., Nicol, K. K., English, B. K., and Liu, Y. (2007) Knockout of Mkp-1 enhances the host inflammatory responses to gram-positive bacteria. *J. Immunol.* **178**, 5312–5320
29. Hammer, M., Echtenachter, B., Weighardt, H., Jozefowski, K., Rose-John, S., Mannel, D. N., Holzmann, B., and Lang, R. (2010) Increased inflammation and lethality of Dusp1-/- mice in polymicrobial peritonitis models. *Immunology* **131**, 395–404
30. Zhang, Y., Zhou, Y., Lou, J., Li, J., Bo, L., Zhu, K., Wan, X., Deng, X., and Cai, Z. (2010) PD-L1 blockade improves survival in experimental sepsis by inhibiting lymphocyte apoptosis and reversing monocyte dysfunction. *Crit. Care* **14**, R220
31. Zhu, W., Bao, R., Fan, X., Tao, T., Zhu, J., Wang, J., Li, J., Bo, L., and Deng, X. (2013) PD-L1 blockade attenuated sepsis-induced liver injury in a mouse cecal ligation and puncture model. *Med. Inflamm.* **2013**, 361501
32. Guignant, C., Lepape, A., Huang, X., Kherouf, H., Denis, L., Poitevin, F., Malcus, C., Cheron, A., Allaouchiche, B., Gueyffier, F., Ayala, A., Monneret, G., and Venet, F. (2011) Programmed death-1 levels correlate with increased mortality, nosocomial infection and immune dysfunctions in septic shock patients. *Crit. Care* **15**, R99
33. Chang, K. C., Burnham, C. A., Compton, S. M., Rasche, D. P., Mazuski, R. J., McDonough, J. S., Unsinger, J., Korman, A. J., Green, J. M., and Hotchkiss, R. S. (2013) Blockade of the negative co-stimulatory molecules PD-1 and CTLA-4 improves survival in primary and secondary fungal sepsis. *Crit. Care* **17**, R85
34. Gordon, S., and Taylor, P. R. (2005) Monocyte and macrophage heterogeneity. *Nat. Rev. Immunol.* **5**, 953–964
35. Parrillo, J. E. (1993) Pathogenetic mechanisms of septic shock. *N. Engl. J. Med.* **328**, 1471–1477
36. Kumar, A., Krieger, A., Symeoneides, S., Kumar, A., and Parrillo, J. E. (2001) Myocardial dysfunction in septic shock: Part II. Role of cytokines and nitric oxide. *J. Cardiothorac. Vasc. Anesth.* **15**, 485–511
37. Dinarello, C. A. (1997) Proinflammatory and anti-inflammatory cytokines as mediators in the pathogenesis of septic shock. *Chest* **112**, 321S–329S
38. Xiao, W., Klement, J. D., Lu, C., Ibrahim, M. L., and Liu, K. (2018) IFNAR1 controls autocrine type I IFN regulation of PD-L1 expression in myeloid-derived suppressor cells. *J. Immunol.* **201**, 264–277
39. Stanciu, L. A., Bellettato, C. M., Laza-Stanca, V., Coyle, A. J., Papi, A., and Johnston, S. L. (2006) Expression of programmed death-1 ligand (PD-L) 1, PD-L2, B7-H3, and inducible costimulator ligand on human respiratory tract epithelial cells and regulation by respiratory syncytial virus and type 1 and 2 cytokines. *J. Infect. Dis.* **193**, 404–412
40. Osum, K. C., Burrack, A. L., Martinov, T., Sahli, N. L., Mitchell, J. S., Tucker, C. G., Pauken, K. E., Papas, K., Appakalai, B., Spanier, J. A., and Fife, B. T. (2018) Interferon-gamma drives programmed death-ligand 1 expression on islet β cells to limit T cell function during autoimmune diabetes. *Sci. Rep.* **8**, 8295
41. Mühlbauer, M., Fleck, M., Schütz, C., Weiss, T., Froh, M., Blank, C., Schölmerich, J., and Hellerbrand, C. (2006) PD-L1 is induced in hepatocytes by viral infection and by interferon-alpha and -gamma and mediates T cell apoptosis. *J. Hepatol.* **45**, 520–528
42. Garcia-Diaz, A., Shin, D. S., Moreno, B. H., Saco, J., Escuin-Ordinas, H., Rodriguez, G. A., Zaretsky, J. M., Sun, L., Hugo, W., Wang, X., Parisi, G., Saus, C. P., Torrejon, D. Y., Graeber, T. G., Comin-Anduix, B., *et al.* (2017) Interferon receptor signaling pathways regulating PD-L1 and PD-L2 expression. *Cell Rep.* **19**, 1189–1201
43. Lu, C., Talukder, A., Savage, N. M., Singh, N., and Liu, K. (2017) JAK-STAT-mediated chronic inflammation impairs cytotoxic T lymphocyte activation to decrease anti-PD-1 immunotherapy efficacy in pancreatic cancer. *Oncoimmunology* **6**, e1291106
44. Morimoto, Y., Kishida, T., Kotani, S. I., Takayama, K., and Mazda, O. (2018) Interferon-β signal may up-regulate PD-L1 expression through IRF9-dependent and independent pathways in lung cancer cells. *Biochem. Biophys. Res. Commun.* **507**, 330–336
45. Lasa, M., Abraham, S. M., Boucheron, C., Saklatvala, J., and Clark, A. R. (2002) Dexamethasone causes sustained expression of mitogen-activated protein kinase (MAPK) phosphatase 1 and phosphatase-mediated inhibition of MAPK p38. *Mol. Cell. Biol.* **22**, 7802–7811
46. Yu, H., Sun, Y., Haycraft, C., Palanisamy, V., and Kirkwood, K. L. (2011) MKP-1 regulates cytokine mRNA stability through selectively modulation subcellular translocation of AUF1. *Cytokine* **56**, 245–255
47. Chen, C. Y., and Shyu, A. B. (1995) AU-rich elements: Characterization and importance in mRNA degradation. *Trends Biochem. Sci.* **20**, 465–470
48. Clark, A., Dean, J., Tudor, C., and Saklatvala, J. (2009) Post-transcriptional gene regulation by MAP kinases *via* AU-rich elements. *Front. Biosci. (Landmark. Ed.* **14**, 847–871
49. Strausberg, R. L., Feingold, E. A., Grouse, L. H., Derge, J. G., Klausner, R. D., Collins, F. S., Wagner, L., Shenmen, C. M., Schuler, G. D., Altschul, S. F., Zeeberg, B., Buetow, K. H., Schaefer, C. F., Bhat, N. K., Hopkins, R. F., *et al.* (2002) Generation and initial analysis of more than 15,000 full-length human and mouse cDNA sequences. *Proc. Natl. Acad. Sci. U. S. A.* **99**, 16899–16903

50. Kovarik, P., Castiglia, V., Ivin, M., and Ebner, F. (2016) Type I interferons in bacterial infections: A balancing act. *Front. Immunol.* **7**, 652
51. Ivashkiv, L. B., and Donlin, L. T. (2014) Regulation of type I interferon responses. *Nat. Rev. Immunol.* **14**, 36–49
52. Bazhin, A. V., von Ahn, K., Fritz, J., Werner, J., and Karakhanova, S. (2018) Interferon-α up-regulates the expression of PD-L1 molecules on immune cells through STAT3 and p38 signaling. *Front. Immunol.* **9**, 2129
53. Hutchins, N. A., Wang, F., Wang, Y., Chung, C. S., and Ayala, A. (2013) Kupffer cells potentiate liver sinusoidal endothelial cell injury in sepsis by ligating programmed cell death ligand-1. *J. Leukoc. Biol.* **94**, 963–970
54. Wang, J. F., Li, J. B., Zhao, Y. J., Yi, W. J., Bian, J. J., Wan, X. J., Zhu, K. M., and Deng, X. M. (2015) Up-regulation of programmed cell death 1 ligand 1 on neutrophils may be involved in sepsis-induced immunosuppression: An animal study and a prospective case-control study. *Anesthesiology* **122**, 852–863
55. Gao, J., Morrison, D. C., Parmely, T. J., Russell, S. W., and Murphy, W. J. (1997) An interferon-gamma-activated site (GAS) is necessary for full expression of the mouse iNOS gene in response to interferon-gamma and lipopolysaccharide. *J. Biol. Chem.* **272**, 1226–1230
56. Song, W., Lu, X., and Feng, Q. (2000) Tumor necrosis factor-alpha induces apoptosis *via* inducible nitric oxide synthase in neonatal mouse cardiomyocytes. *Cardiovasc. Res.* **45**, 595–602
57. Stenzel, W., Soltek, S., Miletic, H., Hermann, M. M., Körner, H., Sedgwick, J. D., Schlüter, D., and Deckert, M. (2005) An essential role for tumor necrosis factor in the formation of experimental murine Staphylococcus aureus-induced brain abscess and clearance. *J. Neuropathol. Exp. Neurol.* **64**, 27–36
58. Rothfuchs, A. G., Gigliotti, D., Palmblad, K., Andersson, U., Wigzell, H., and Rottenberg, M. E. (2001) IFN-alpha beta-dependent, IFN-gamma secretion by bone marrow-derived macrophages controls an intracellular bacterial infection. *J. Immunol.* **167**, 6453–6461
59. Lázár-Molnár, E., Gácser, A., Freeman, G. J., Almo, S. C., Nathenson, S. G., and Nosanchuk, J. D. (2008) The PD-1/PD-L costimulatory pathway critically affects host resistance to the pathogenic fungus Histoplasma capsulatum. *Proc. Natl. Acad. Sci. U. S. A.* **105**, 2658–2663
60. Roussey, J. A., Viglianti, S. P., Teitz-Tennenbaum, S., Olszewski, M. A., and Osterholzer, J. J. (2017) Anti-PD-1 antibody treatment promotes clearance of persistent cryptococcal lung infection in mice. *J. Immunol.* **199**, 3535–3546
61. Whibley, N., Jaycox, J. R., Reid, D., Garg, A. V., Taylor, J. A., Clancy, C. J., Nguyen, M. H., Biswas, P. S., McGeachy, M. J., Brown, G. D., and Gaffen, S. L. (2015) Delinking CARD9 and IL-17: CARD9 protects against Candida tropicalis infection through a TNF-α-dependent, IL-17-independent mechanism. *J. Immunol.* **195**, 3781–3792
62. Tsiodras, S., Samonis, G., Boumpas, D. T., and Kontoyiannis, D. P. (2008) Fungal infections complicating tumor necrosis factor alpha blockade therapy. *Mayo Clin. Proc.* **83**, 181–194
63. Triantafyllou, E., Gudd, C. L., Mawhin, M. A., Husbyn, H. C., Trovato, F. M., Siggins, M. K., O'Connor, T., Kudo, H., Mukherjee, S. K., Wendon, J. A., Bernsmeier, C., Goldin, R. D., Botto, M., Khamri, W., McPhail, M. J., *et al.* (2021) PD-1 blockade improves Kupffer cell bacterial clearance in acute liver injury. *J. Clin. Invest.* **131**, e140196
64. Dorfman, K., Carrasco, D., Gruda, M., Ryan, C., Lira, S. A., and Bravo, R. (1996) Disruption of the erp/mkp-1 gene does not affect mouse development: Normal MAP kinase activity in ERP/MKP-1-deficient fibroblasts. *Oncogene* **13**, 925–931
65. Kim, V. Y., Batty, A., Li, J., Kirk, S. G., Crowell, S. A., Jin, Y., Tang, J., Zhang, J., Rogers, L. K., Deng, H. X., Nelin, L. D., and Liu, Y. (2019) Glutathione Reductase promotes fungal clearance and suppresses inflammation during systemic Candida albicans infection in mice. *J. Immunol.* **203**, 2239–2251
66. Wang, X. X., Zhao, Q., Matta, R., Meng, X. M., Liu, X. P., Liu, C. G., Nelin, L. D., and Liu, Y. S. (2009) Inducible nitric-oxide synthase expression is regulated by mitogen-activated protein kinase phosphatase-1. *J. Biol. Chem.* **284**, 27123–27134
67. Lee, S. Y., Buhimschi, I. A., Dulay, A. T., Ali, U. A., Zhao, G., Abdel-Razeq, S. S., Bahtiyar, M. O., Thung, S. F., Funai, E. F., and Buhimschi, C. S. (2011) IL-6 trans-signaling system in intra-amniotic inflammation, preterm birth, and preterm premature rupture of the membranes. *J. Immunol.* **186**, 3226–3236
68. Aparicio-Vergara, M., Tencerova, M., Morgantini, C., Barreby, E., and Aouadi, M. (2017) Isolation of Kupffer cells and hepatocytes from a single mouse liver. *Methods Mol. Biol.* **1639**, 161–171